SAPIENZA
UNIVERSITÀ DI ROMA

Analysis of conduction velocity from High-Density surface EMG as indicator of muscle fatigue during robot-mediated ankle movements

Dipartimento di Ingegneria informatica automatica e gestionale

Corso di Laurea Magistrale in Artificial intelligence and Robotics

Candidate

Giovanni Corvini
ID number 1719710

Thesis Advisor

Febo Cincotti

Co-Advisor

Juan C. Moreno

Academic Year 2018/2019

Thesis defended on July 2019
in front of a Board of Examiners composed by:

Prof. Fiora Pirri (chairman)
Prof. Aris Anagnostopoulos
Prof. Febo Cincotti
Prof. Pierangelo Di Sanzo
Prof. Umberto Nanni
Prof. Alessandro Pellegrini
Prof. Aurelio Uncini

Analysis of conduction velocity from High-Density surface EMG as indicator of muscle fatigue during robot-mediated ankle movements
Master thesis. Sapienza – University of Rome

This thesis has been typeset by LaTeX and the Sapthesis class.

Version: July 18, 2019

Author's email: gio.corvini@gmail.com

To my beloved Lulù,

to my family,

to me.

Abstract

Rehabilitation Robotics has the objective of enhancing medical rehabilitation through the use of robotic systems, like exoskeletons. Generally, these systems present adaptive control in order to improve the human-robot interaction in all circumstances, but they do not take into account physiological muscles changes in the users. In this work, the analysis of myoelectric parameters as manifestation of muscle fatigue was performed in lower limb muscles. During the robotic training paradigm, which has been previously established, we investigated the muscle fatigue that could be present during the motor task through the use of a Motorized Ankle Foot Orthosis. All data have been acquired through the High-Density surface electromyography technique. In the first study, co-contraction indexes were computed during contractions of the tibialis anterior (dorsiflexion) and of the gastrocnemius (plantarflexion). Such indexes were evaluated as possible measures of muscle fatigue but the result of this analysis showed that co-contraction based indexes are not related to fatigue. In the second study, the dorsiflexion was analyzed in two experiments: one with a long lasting contraction and one with repetitive contractions. The innovative Decomposition of Multichannel Surface Electromyograms software was used in order to decompose the signals and to extract Motor Units activity. Then, the conduction velocity was computed at muscle fiber level and at motor unit level, and a significant correlation ($\rho = 0.67$ and $p < 0.0001$) between these two measures was found. Two different experiments were performed and compared to evaluate the muscle fatigue process. Finally, the conduction velocity and other electromyography descriptors were examined, showing the feasibility of using these parameters to assess muscle fatigue.

Acknowledgments

First of all, I am particularly grateful to my parents and sisters that made many sacrifices to let me achieve this goal, being always by my side and supporting me despite my mistakes. Then, I would like to thank my bro, Cristian, who puts up with me since we were born. Moreover, I would like to thank Giulia, Federico, Enrico and all friends that have always been there when I needed them. Afterward, I should thank Roberto, Andrea, Mekki and many other friends that I met at university, who taught me a lot during these years. I wish to acknowledge the opportunity of working at the Cajal Institue in Madrid provided by José L. Pons, and I would like to express my gratitude to my advisor Febo Cincotti, my co-advisor Juan C. Moreno, the professor Ales Holobar and all the neurorehabilitation group for their help. A particular thanks goes to Guillermo, an incredible tutor that provided me helpful advice and motivated me to do my best all the time. I wish to thank Martina and Delfina, wonderful girls that were my family in Madrid, with whom I spent one of the most important parts of my life. Finally, my special thanks go to Alice, an extraordinary girl that really changed my life and, hopefully, she will continue to do it.

Contents

List of Abbreviations

AMVC	Approximated Maximum Voluntary Contraction
ARV	Average Rectified Value
BBB	BeagleBone Black
CI	Co-contraction Index
CPU	Central Processing Unit
CV	Conduction Velocity
DEMUSE	Decomposition of Multichannel Surface Electromyograms
DRL	Driven Right Leg
gCKC	gradient Convolutional Kernel Compensation
CWT	Continuous Wavelet Transform
ECG	Electrocardiogram
EMG	Electromyography
FEM	Finite Element Method
GM	Gastrocnemius Medialis
GUI	Graphic User Interface
IDR	Instantaneous Discharge Rate
IED	Interelectrode distance
IPT	Innervation Pulse Train
IZ	Innervation Zone
JASA	Joint Analysis of EMG spectrum and Amplitude

LLC	Long Lasting Contraction
MACCEPA	Mechanically Adjustable Compliance and Contrallable Equilibrium Position Actuator
MAFO	Motorized Ankle Foot Orthosis
MDF	Median Frequency
MFL	Muscle Fatigue Level
MFCV	Muscle Fiber Conduction Velocity
MLE	Maximum Likelihood Estimation
MNF	Mean Frequency
MSE	Mean Square Error
MU	Motor Unit
MUAP	Motor Unit Action Potential
MUAPT	Motor Unit Action Potential Train
MUCV	Motor Unit Conduction Velocity
MVC	Maximum Voluntary Contraction
PLI	Power Line Interference
PNR	Pulse Noise Ratio
RC	Repetitive Contraction
RMS	Root Mean Square
RQA	Recurrence Quantification Analysis
SNR	Signal to Noise Ratio
SPU	Secondary Processing Unit
TA	Tacit Adaptability
TBA	Tibialis Anterior
VSA	Variable Stiffness Actuators
WR	Wereable Robot

Introduction

In the last years, the use of Wearable Robots (WRs) has dramatically increased. The goal of these robotic devices is a physical and cognitive interaction with the user to improve the human life quality. WRs are technologies aimed at extending, complementing, substituting or enhancing human functions and capabilities. They may operate alongside human limbs, as in the case of orthoses and exoskeletons, or they may substitute for missing limbs after an amputation, as in the case of prosthesis. Lower-limb orthoses are mechanical structures that map on to the anatomy of the human limbs and, as like exoskeletons, are usually used in rehabilitation therapies; one of their main purposes is to restore weak or lost motor functions to their natural level. In order to monitor the motor function of the subjects, in many works the myoelectric activity has been used as input parameter of the robotic control system. Since the robotic devices should interact with the human under different circumstances, there has been a growing will to design new machine learning and adaptive methods, such as artificial neural networks, reinforcement learning or adaptive controls. A frequent choice of the control strategy in WRs falls on adaptive controllers, so that systems can automatically compensate for variations in their dynamic and maintain at optimum level their performance. Besides, in the last few years, researchers are developing new advanced techniques, making systems able to produce consistent actions in response to complex environmental changes, e.g. tacit learning. Recently, G. Asin Prieto et al. presented the concept of "Tacit Adaptability" (TA), which is a symbiotic control strategy based on biomimetic mechanism. Their research, within the European project BioMot, focused on the development of an exo capable of interacting with the user by modifying its compliance. A PID torque controller with a TA module was implemented in all the joints.

In this work, a single joint, namely the Motorized Ankle Foot Orthosis (MAFO), was used. The robotic platform allows to exert controlled torque profiles to the ankle joint of the user and it was used in some experiments with healthy subject to improve the human-robot interaction, so as to do another step towards the final goal, that is to translate this robotic system into a rehabilitative tool. The idea of a long-term project was to improve the existing control strategy of this MAFO system, modulating its controller by using myoelectric information. So, this thesis aim to find an indicator of muscle fatigue to update the behaviour of the controller. In this way, the force exerted by the robot during specific exercises should be modulated by physiological parameters of the user, so as to make a rehabilitation therapy safer. Therefore, this work focused on the analysis of some variables in order to assess the fatigue in lower limb muscles. Some background information on the muscle physiology and the EMG are given in Chapter 1. Then, a detailed description of the experimental platform is provided in Chapter 2. The experiments are presented in the third Chapter. Initially, several Co-contraction Indexes (CIs) were studied and implemented. Data were acquired from lower limb muscles in a bipolar electrode configuration during cyclic static contractions. Then, the conduction velocity, through the High-Density surface EMG technique, was investigated. This variable was computed both at global level (muscle fiber) and at local level (motor unit). The extraction of motor unit was done through the use of an innovative technique, Decomposition of Multichannel Surface Electromyograms (DEMUSE). Two different exercise were proposed to evaluate muscle fatigue in the tibialis anterior. The first was a long lasting contraction, while the second one consisted of repetitive contractions. In Chapter 4 we analyzed the results. Some relations between the Muscle Fiber Conduction Velocity (MFCV), and the mean and median of Motor Units Conduction Velocity (MUsCV) were investigated. Some EMG descriptors were computed and considered for validating the results obtained. The time evolution of the mean of the extracted MUs was evaluated. Moreover, firing of each MUs were compared between the two different exercises and between two subjects. Finally, the conclusions are given in Chapter 5, explaining how the muscle fatigue was assessed through the CV.

Chapter 1

Muscle physiology and activity

The human body contains several types of muscle tissue that, despite any outward similarities, are different in their biomechanics and their uses in the body. The three primary types of muscle tissue are: smooth, cardiac and skeletal muscle. They are composed by two proteins, actin and myosin, responsible for the contracting process. The contraction takes place when muscle plasma membranes change their electrical states from polarized to depolarized; this process is called excitability. During a depolarization, an electrical wave is generated, known as action potential, and it is sent along the entire length of the membrane. While the skeletal muscle completely depends on signalling from the nervous system, both cardiac and smooth muscles can also respond to other stimuli, like hormones or local stimuli. Muscle presents the property of contractility, which allows muscle fibers to shorten their length; instead, when the muscle relaxes, muscle fibers return to their original length thanks to their elasticity. Finally, despite these properties, muscle tissues are also capable of stretching and extending, a quality known as extensibility [1],[2]. Although the three types of muscle tissues share some properties, they differ both at macroscopic level, namely in their functionality, and at microscopic level, that is their protein organization structures. Therefore, the three different macro-groups are:

1. Smooth muscle, which is a type of non-striated muscle that can be found in different parts of the body, from arteries and veins to reproductive, gastrointestinal or respiratory tracts. It is called smooth since the actin and myosin are not arranged in regular patterns, like in the other tissue types.

Its main function is to regulate the size of intestinal muscles and glands for the contractions of the intestinal tract, known as peristalsis. Its contractions are involuntary.

2. Cardiac muscle, which is the most important muscle of our body because it propels blood both inside the circulatory system through the arteries and into the heart through the veins. It is a striated muscle tissue since actin and myosin proteins are arranged in a regular way inside the cytoplasm of individual muscle cell, creating patterns or stripes called striations. Moreover, cardiac muscle fibers have one to two nuclei and they are connected to each other so that the entire heart contracts as one unit, differently from skeletal muscle fibers. Its contractions are primarily involuntary.

3. Skeletal muscle tissue is a striated muscle like the cardiac one, but it has very different characteristics. It is found attached to bones, skin, fascia, and other muscles. The central structure of the skeletal muscle is composed by multi-nucleated fibers and its role is to hold posture and to produce body movements by means of forces applied to bones and joints. The main difference with the other muscle tissues resides in the contraction because in this case it is voluntary, since it is activated by the human decision.

1.1 Skeletal Muscle

Skeletal muscle is one of the most dynamic and plastic tissues of the body and it contains 50-75% of all body proteins covering 40% of the total weight in humans. Its primary function is to maintain posture, stabilize bones and joints, control internal movements and generate heat. Every skeletal muscle consists of various integrated tissues, like skeletal muscle fibers, blood vessels, nerve fibers and connective tissues [3]. Each muscle has three layers of connective tissue, called mysia, that encloses it and provides structure to the muscle. Each single layer is wrapped inside a connective tissue, called epimysium, that allows muscles to contract and to move while maintaining their integrity. Inside a single muscle cell, there are several parallel bundles of skeletal muscle fibers, called fascicles, wrapped up in a smooth connective

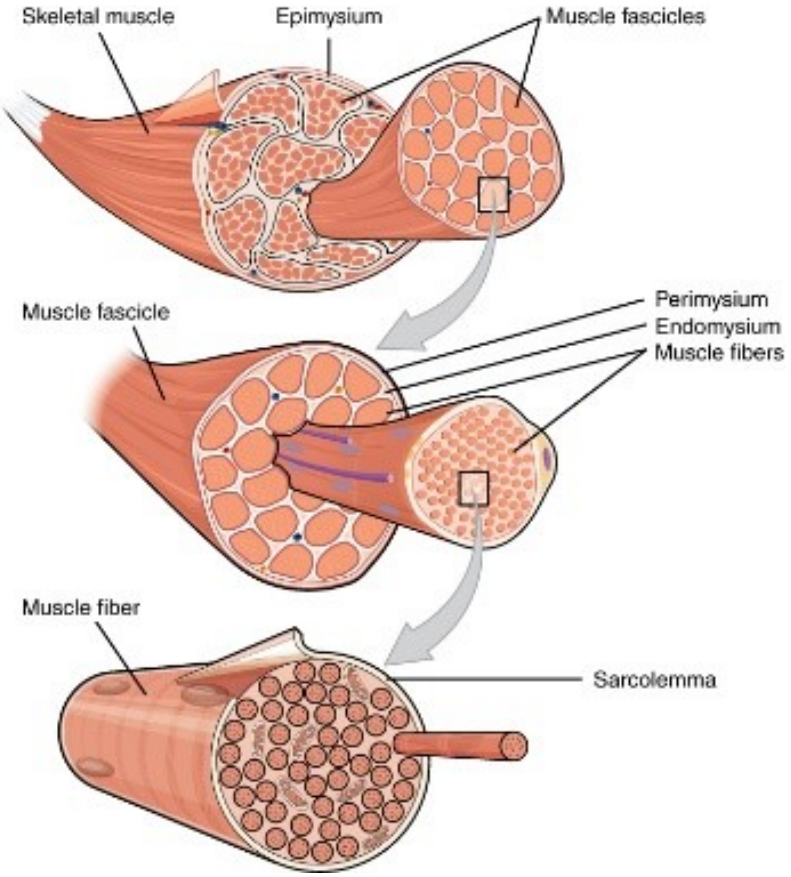

Figure 1.1. Internal structure of a skeletal muscle.

tissue, known as perimysium. As shown in Figure 1.1, the fibers are multi-nucleated, that means they contain many myofibrils which are wrapped inside a cell membrane called sarcolemma and they contain, in turn, myofilaments. Myofibrils have distinct, repeating microanatomical units, called sarcomeres; each sarcomere is like a three-dimensional cylinder long approximately 2 μm delimited by structures called Z-discs or Z-line, to which the actin myofilaments are anchored, as can be seen in Figure 1.2. Inside the sarcomere, different types of myofilaments are present: thick, thin, and elastic filaments. The actin, tied to troponin and tropomyosin proteins, is thinner than myosin; for this reason it is known as thin filament of the sarcomere. Conversely, myosin strands and their multiple heads represent the thick filament of the sarcomere since they have more mass and are thicker. These protein filaments give the muscle its striated appearance. Elastic filaments are made of titin, a large

springy protein. They run through the core of each thick filament and they anchor it to the Z-line, which is the sarcomere end point. Moreover, titin protein stabilizes the thick filament, by preventing overstretching of the thick filament, and it recoils like a spring whenever a muscle is stretched. During muscle contraction, the heads of the myosin filaments attach to thin filaments and pull them past one another. The action of myosin attachment and actin movement results in sarcomere shortening. Therefore, muscle contraction consists of the simultaneous shortening of multiple sarcomeres, but in order to activate the these movements within the fibers, an excitation signal from the motoneuron is required.

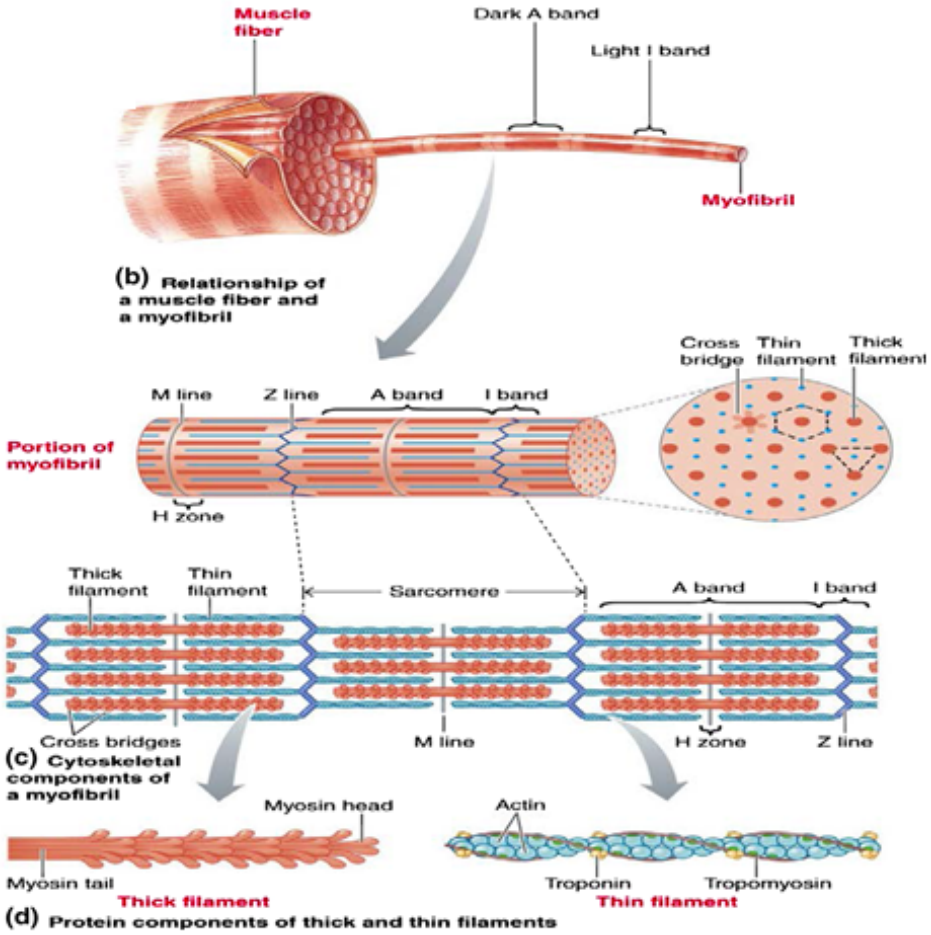

Figure 1.2. Internalstructure of a single myofibril inside a muscle fiber. Taken from [3]

1.2 Physiology of Motor control

The central nervous system is organized in a hierarchical way. Motor programming tasks, in fact, start from different parts of the brain such as premotor cortex, supplementary motor area, cerebellum and other areas. The inputs sent from these parts converge to the primary motor cortex, exciting or inhibiting different neurons in the primary motor area. Thus, these neurons in the primary motor cortex send sensory and other inputs to the interneurons, and therefore to the motoneurons located in the ventral horn of the spinal cord or the brain stem.

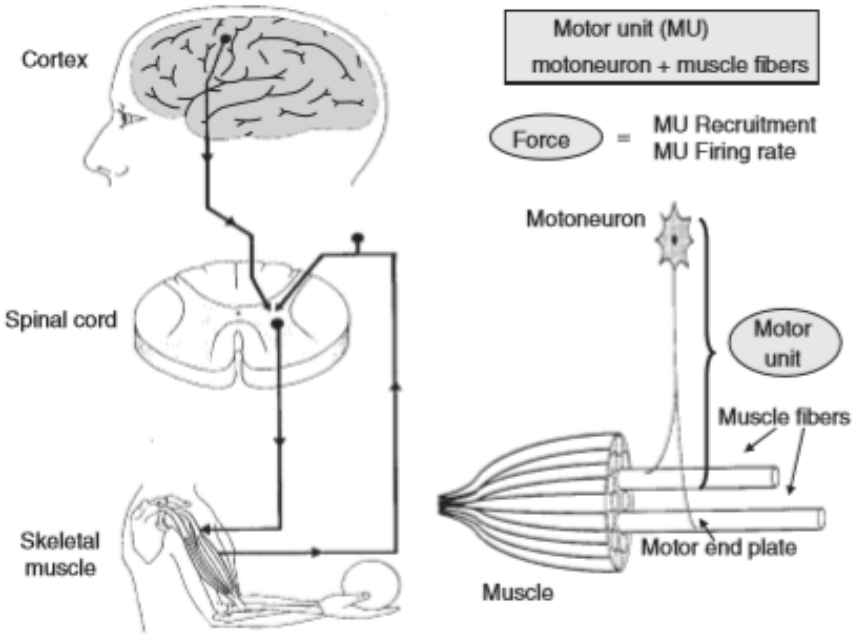

Figure 1.3. Schematic representation of motor control mechanisms and of the motor units and its components. Taken from [4]

Here, the axon of each motor neuron comes out of the brain stem through a cranial nerve, or out of the spinal cord through the ventral root, and it projects in a peripheral nerve to all the muscle fibers that it innervates, as it is possible to see the higher resolution image attached in Figure 1.3 [4].

1.2.1 Motor Unit

A motor unit consists of an α-motoneuron in the spinal cord and all the muscle fibers it innervates. This motoneuron represents the sum of every descending and reflex input, determining the firing pattern and thus the activity of the MU. The size of a motor unit depends on the nature of the muscle. Generally, small motor units innervate a few muscle fibers and allow very precise movements, like eye movements for focusing or finger movements for grasping. On the other hand, large motor units can innervate up to thousands of fibers producing simple and powerful movements, e.g. the extension of the knee. Since small motor units have a lower threshold with respect to large motor units, they are usually activated earlier [5]. Each motor unit can generate a variable force depending on the average cross-sectional area of the muscle fibers (μm^2), on the specific force of the fibers ($mN/\mu m^2$) and mainly on the fiber innervation number. Due to the exponential distribution of innervation number across a motor unit pool, it's worth noting that there exist a difference between the number of motor unit action potentials, denoted as "neural drive", discharged from the spinal cord and the number of muscles fiber action potentials, indicated as "muscle activation", recorded in the muscle with EMG electrodes. Generally, the force produced in a contraction relies on several MUs, from one hundred to thousands according to the muscle size, especially during long sustained or explosive contraction. Moreover, even if it is difficult to achieve a motor units classification based on their physiological properties, three different types of motor unit have been identified in earlier studies:

1. fast twitch, fatigable (FF or type IIB);
2. fast-fatigue-resistant (FR or type IIa);
3. slow-twitch (S or type I), which is most resistant to fatigue.

In order to study MU behaviour, classical intramuscular electrodes are required, but recently new techniques, e.g. high density surface EMG, have been developed in order to evaluate MU from surface electrode [6]. Contrary to intramuscular recordings, the number of motor units recorded with surface EMG strongly depends on the number of electrodes used.

1.2.2 Recruitment order and rate coding

The muscle force, during voluntary contractions, is strongly dependent by a combination of two variables: the recruitment order and the firing frequency, also known as rate coding. Henneman et al. [7], who obtained results from cat motoneurons, defined the "size principle" since it was found that, during muscle contraction, the recruitment order was related to the motoneuron and MU size. Studies of motor unit recruitment during voluntary contraction in humans using EMG techniques has been done in [8]. In fact, the smaller ones have a lower threshold and are activated first, while the larger ones have a higher threshold and they are activated afterwards. So, based on many data supporting this theory, the recruitment order of the motor units is well-known as "normal sequence of recruitment" or "orderly recruitment". Moreover, through several studies, it has been stated that the rate coding and the MU recruitment rely on muscle force and on the speed of contraction; Kukulka and Clamann, Moritani et al. demonstrated that for some muscles composed of type I fiber (slow-twitch), the force modulation is dependent on the firing frequency, while for muscle group composed by both type I and II fibers, the force modulation is mainly dependent on the MU recruitment [9]. Therefore, the electrical activity in a muscle, and consequently the force produced, is predominantly determined by the number of MUs recruited and by their mean discharge frequency. For this reason, it has been evinced that, under certain experimental conditions, there exists a direct relationship between the electromyogram and the exerted force.

1.2.3 Muscle Fatigue

Muscle fatigue occurs in everyday life and it can be described as a muscle pain or a decrease in performance during physical activities. The fatigue process accounts for all the physiological changes taking place within a muscle and it starts evolving at the beginning of the contraction [1]. At muscular level, it reflects a progressive reduction of force produced by muscle fibers. More generally, the fatigue process arises from potential sites, e.g. in the neuromuscular system, the motor cortex, the excitatory drive, the α-motoneurons, the neuromuscular transmission and some others [6], [4]. Since, during fatigue, several factors affect the EMG signals, the

majority of the fatigue assessment have been done during isometric constant force conditions [10] [11]; nevertheless, there also exists studies about fatigue evaluation during dynamic contractions [12], [13], [14]. It has been noted that before the force decrease, it is present an alteration in the muscle electrical properties, commonly known as myoelectric manifestations of muscle fatigue. Since the electromyographic signals are more and more used in biomedical fields, e.g. control of prostheses or rehabilitation, research has have been conducted trying to characterize these myoelectric manifestations of fatigue from surface EMGs, both in time and frequency domain. Recently, a considerable review has been done, gathering multi-channel approaches to the study of myoelectric manifestations of muscle fatigue [15]. In the time domain, the main visible change in the EMG is an increase of the signal amplitude due to muscular effort, while in the frequency domain, the dominant change is a compression of the signal spectrum towards lower frequencies. According to several studies (Lindstrom and Magnusson 1977, De Luca 1984, Arendt-Nielsen and Mills 1985), the effect of CV reduction, which was associated symptom of muscle fatigue, on spectral and amplitude variables of surface EMG is well established [16]; therefore, until now, the Root Mean Square (RMS), the Average Rectified Value (ARV), and the Mean Frequency (MNF) and the Median Frequency (MDF) are considered the principal indices of muscle fatigue. The relationship between muscle fatigue and these metrics have been fully examined in [17]. Furthermore, a new method to quantitatively estimate muscle fatigue from surface electromyography has been recently proposed, that is to use the ratio between MNF and ARV as index of muscle fatigue; this method produced a muscle fatigue assessment more correctly compared with the conventional methods [18]. Besides these, in order to best describe the EMG descriptor changes during muscle fatigue, several methods were developed such as recurrence quantification analysis (RQA) [4], the Fourier-based spectral estimators, the joint analysis of EMG spectrum and amplitude (JASA), time-varying autoregressive approaches, time-scale methods, wavelet analysis and so on [15]. In addition, the conduction velocity (CV) was found to be a good parameter for muscle fatigue assessment; in fact, since CV and muscle effort are related, extensive studies were conducted in this direction.

Conduction Velocity

Conduction velocity is defined as the propagation velocity of depolarization along the muscle fibers [16]. It reflects the membrane muscle fibre properties, and thus it can be used as an indication of the physiological or pathological state of the muscle fiber membrane. It is related to the type and diameter of muscle fibres [19], ion concentration, pH and motor unit firing rate. Ideally, the surface action potentials detected along the muscle fibers travel without changes in shape from the innervation zone of the motor unit to the tendon endings, but it never happens in practice. Thus, there is not a unique mathematical definition of the delay between detected potentials and different estimation methods were developed [20]. Some of them have been collected in a review [21]; the main difference found among these methods relies on the number of the electrode used for the detection: from a single or bipolar electrodes to electrode array and matrix. Nowadays, a growing interest is going towards non invasive multi-channel approaches, since they allow more reliable results, both at global level, e.g. Muscle Fiber Conduction Velocity (MFCV), and at local level, e.g Motor Unit Conduction Velocity (MUCV) or Motor Unit Action Potential Conduction Velocity (MUAPCV) [22], [23], [24], [25], [26], [27]. In fact, the analysis of motor unit CV is made possible thanks to innovative methods for the MU decomposition from high density surface EMG [28], e.g. matched Continuous Wavelet Transform (CWT) [29], convolutive blind source separation [30], [31], [32].

1.3 Electromyography

The electromyography (EMG) is the study of the electric potential fields generated by the depolarization of the outer muscle fibre membranes (the sarcolemma). The EMG signal is generated by the electrical activity of all muscle fibers that are active during a contraction. The sources of the signal are separated from the recording electrodes by several muscle tissue that, even if they are conductive, act as spatial and temporal low-pass filter on the potential distribution. Thus, the EMG signal represents the anatomical and physiological properties of muscles. Nevertheless, the signal recorded is usually a composition of many signals, generally altered by the

presence of noise. There exist different types of noise, that depend on several factors and they will be investigated more in detail in the following subparagraphs.

1.3.1 Mathematical model of EMG signal

In order to define a mathematical model of the EMG, it is possible to start from the electrical impulse sent from the motoneuron to the all muscle fibers that it innervates, generating Muscle Fiber Action Potentials (MFAPs) [33]. The sum of all the MFAPs activated by a single MU is called Motor Unit Action Potential and it is given by the formula:

$$MUAP_j(t) = \sum_{i=1}^{n} MFAP_i(t - \tau_i)s_i \tag{1.1}$$

where n is the number of the muscle fibers in the j^{th} Motor Unit of a contracting muscle, τ_i is the temporal delay of $MFAP(t)$ and s_i is a binary variable that indicate if the i^{th} Muscle Fiber fires (value 1) or it does not (value 0). Then, the sum of all the MUAPs generated by a single Motor Unit produce a Motor Unit Action Potential Train, according to the equation:

$$MUAPT_j(t) = \sum_{k=1}^{M} MUAP_{jk}(t - \delta_{jk}) \tag{1.2}$$

where M is the number of times that the j^{th} MU fires, δ_{jk} is the k^{th} firing time of MU_j and $MUAP_{jk}(t)$ is the k^{th} $MUAP$ generated by MU_j during its k^{th} firing. Finally, all the MUAPTs produced by each Motor Unit sum up together in order to generate the whole signal, represented like EMG signal, given by:

$$EMG(t) = \sum_{i=1}^{N} MUAPT_j(t) + n(t)) \tag{1.3}$$

Where N is the number of active MUs, $MUAPT_j(t)$ is the train of MUAP generated by the j^{th} Motor Unit and $n(t)$ is the sum of the noises inside the signals.

1.3.2 Signal generation and detection

The resting potential of the muscle fibre membrane is around $-70/-90$ mV, negative inside the cell with respect to extracellular zone. This resting potential is kept constant using the sodium-potassium pump that works against the concentration gradient of ions flowing through the membrane. Therefore, when an action potential, sent from the motoneuron, reaches the neuromuscular junction, acetylcholine is released in the gap between the nerve terminal and the motor end plate, producing the opening of the sodium channels; at this point, the ions (Na+) enter inside the membrane creating a membrane depolarization that triggers an action potential, subsequently spread along the entire muscle length until the tendon. Thus, the muscle fibre membrane depolarization generates an electric field that can be easily recorded through some detecting tools called electrodes. The electric field generated by the muscle fibre membrane depolarization can be recorded in two different ways:

- internally by using intramuscular electrodes.
- externally by applying surface pair of electrodes,

More advanced techniques are now widely used in research laboratories that are based on the simultaneous use of both types of electrode, while others are based on multichannel detection, known as High-Density surface EMG (HD-sEMG).

1.3.3 Intramuscular electrodes

Typically needle or wire-based intramuscular electrodes, like in Figure 1.4, are used when the muscle activity to be studied is small or located deep inside the body. In fact, a monopolar EMG needle can record from a spherical volume even a couple of millimetres in radius around the needle tip. By inserting electrodes into the muscle tissue through the skin, the detection of electric potentials is strongly accurate and precise because it is very close to the generation source; furthermore, the signal is minimally influenced by the different skin layers and by the activity of muscles located nearby. Intramuscular electrodes, besides to identify voluntary contractions or fasciculation (involuntary twitch), are able to detect also fibrillations, which are isolated spontaneous activation of individual muscle fibers.

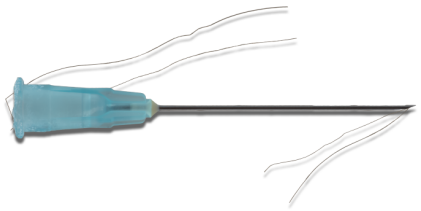

Figure 1.4. Couple of thin wire electrodes with insertion needle.

Such potentials are very important because they are a sign of denervation and cannot be detected with surface electrodes. Moreover, using intramuscular electrodes, it is possible to identify also changes in motor unit size and in their internal structure. It is meaningful to detect these changes because they can reveal abnormal function or some pathological disorders. For example, in presence of neurogenic disorders, some motoneurons degenerate, while the surviving ones tend to grow, resulting in a much denser and larger motor unit. Another example is when a motor unit may lose some of its muscle fibers due to various disease processes and thus it could become smaller. Thus, the aim of using intramuscular recording techniques is to study the physiology and pathology of the MU. Despite all these benefits, The needle cannot simultaneously record potentials from all muscle fibers in a motor unit, that could be up to several hundred. Moreover, slight needle movement inside the muscle could result in different muscle fiber acquisition within the same MU. Since it records on a small fraction of the muscle, occasional false negative results could be encountered. In addition, this acquisition technique must be avoided in some applications like sport, rehabilitation or occupational medicine, where the assessments must be repeated frequently and this kind of invasive electrodes is not acceptable [34].

1.3.4 Surface electrodes

Surface electrode is a non-invasive technique used for recording muscle electrical activity applying one or more electrodes (see Figure 1.5) on the skin, exactly over the muscle region of interest. They are usually better suited for studying the activities of a single muscle or muscle groups, e.g. the temporal and frequency pattern,

the behaviour under specific conditions or the fatigue processes. Modern surface electrode arrays or matrices also allow the mapping of the MUAP propagation from the innervation zone to the tendon endings, giving high-accuracy estimation of location of the innervation zone, length and orientation of the fibers or, as deeply analysed in this work, muscle fiber conduction velocity.

Figure 1.5. Bipolar electrrodes 15x15mm with concentric connector.

Nevertheless, the signal extracted from the EMG strongly depends on many aspects, such as the location, the interelectrode distance (IED), the size and the position of the electrodes along the fiber direction. With respect to the intramuscular, they are easier to apply because are risk-free; in fact, surface electrodes are widely used in each field application, like research, sport or daily activities in hospitals. But, besides being less accurate than intramuscular electrodes, the greater drawback of surface EMG technique resides in the signal quality because it is generally affected by different kinds of noise. So, there exists a variety of surface electrodes and the right electrode type must be chosen according to the specific features the user wants to analyse. In this work surface electrodes technique have been used, in particular the High Density surface EMG, an innovative technique that allows the acquisition of a large number of channels.

Electrode–Skin Impedance

The electrode-skin contact is intrinsically noisy and it varies its impedance depending on the electrode material and size as well as the gel and skin condition. In order to reduce the impedance as much as possible, a gelled contact is preferred, even if during long term recordings, the gel could dry changing the skin properties.

Piervirgili et al. [35] investigated the effects of skin treatments on the impedance. It was found that no statistical difference exists between no treatment, rubbing with alcohol or stripping several times with commercial office-type adhesive tape, while they discovered that washing with soap makes the impedance lower, and rubbing with abrasive conductive paste and rinsing is the most effective treatment for lowering the impedance and reducing the Power Line Interference (PLI). The impedance is also affected by the electrode material. Generally, they are classified in polarizable and nonpolarizable electrode. Polarizable ones (e.g. gold, platinum or iridium electrodes) are characterized by capacitive behaviour because only displacement current passes between the skin and electrode. On the other hand, non-polarizable electrodes (e.g. galvanized and sintered silver/silver chloride (Ag/AgCl) electrodes) behave like resistors since they allow a free flow of charge across the electrode-skin interface. For the use of surface EMG non-polarizable electrodes are preferred since they are highly steady, while polarizable ones show high sensitivity to movement artefacts.

Inter-Electrode Distance

The Inter-Electrode Distance (IED) shows the effective distance between two adjacent electrodes. Generally, the muscle volume considered by the recording system is a sphere whose radius equals the IED. Thus, the larger the inter-electrode distance, the wider the pick-up volume sampled, which implies higher amplitude of the signal but less spatial specificity.

Electrode placement

The right location of surface electrodes is important for having an accurate evaluation of the muscle activation [36] and for improving the Signal-to-Noise Ratio (SNR) of sEMG signals. The electrodes are separated from the muscle by a layered volume conductor consisting of the skin and subcutaneous tissues (adipose tissue and other soft tissues), like in Figure 1.6. These tissues act as spatial low pass filters smoothing the amplitude and the frequency content of detected MUAPs. Hence, since the action potentials from motoneurons are propagated along muscle fibers, the electrodes should be aligned along these fibers and far from the tendons; in addition, for stable

EMG signals, it is suggested that electrodes should be placed at a sufficient distance from the innervation zone (IZ), that is the location from which starts the impulse propagation. Finally, in muscles with irregularly oriented muscle fibers, such as pennate muscles, it is not easy to determine the proper direction of fibers, and thus the right position of the electrodes. In this case, for investigating the activity of these muscles, it would be preferable to choose intramuscular EMG, but if this is not possible, it is important to consider these limitations regarding the optimum surface electrode locations and consequently, regarding the quality of the signals.

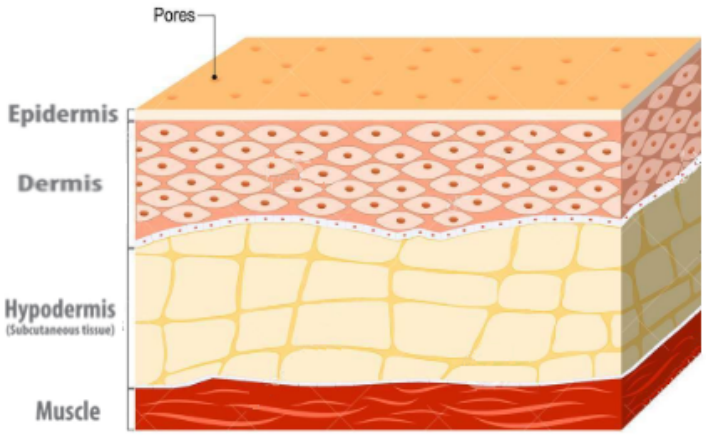

Figure 1.6. The structure of the skin.

1.3.5 Noise sources in EMG signal

The EMG signals depend on several aspects like the internal structure of the subject, the individual skin formation, the blood flow velocity, the measured skin temperatures, the tissue structure, the electrodes placement, and so on. Besides physiological factors, the EMG signals are also affected by noises of different nature that could bring to a wrong EMG analysis or to a wrong feature extraction. The noise found in EMG has multiple causes, but often it is possible to completely remove some components in order to reduce it. Hence, various denoising methods were developed to face with some specific causes of noise [37].

Inherent noise in electronics equipment

During acquisition, all types of electronic equipment generate electrical noise, often called "inherent noise". This noise has frequency components that goes from zero Hertz to several thousand and it cannot be eliminated, but only reduced by using high-quality components and intelligent circuit design.

Movement artefact

Movement artefacts are usually produced when cables move during the connection to the amplifier and it can be easily reduced minimizing the movements by fixing the cables. When a muscle contracts, all its fibers length decrease, generating some small movements of the skin and, consequently, of the electrodes. This generated noise has a frequency range of 1-10 Hz with a voltage amplitude similar to that of the EMG. It can be efficiently removed by recessing the electrode in a cup of electrolytic fluid or gel. Therefore, movement of the skin may affect the electrolyte, but not the electrode recessed in the cup. Another kind of artefact is typically caused by the potential difference between skin layers. Tam and Webster [38] studied how the skin abrasion could improve the quality of biopotential signals. Even if the use of skin abrasion is controversial due to the potential dangers that could cause to the skin, it has been found that a fine abrasion is effective in minimizing motion artefact.

Electromagnetic noise

The main source of this noise is the electromagnetic radiation. The amplitude of this kind of noise varies from one to three times that of the desired EMG signal. Since the human body is constantly exposed to these electromagnetic radiations, it is always present. The dominant ambient noise is called Power-Line Interference and it has a frequency of 50 Hz in Europe (60 Hz in USA), coming from all the power sources. It can be removed using a band-stop filter, known as notch filter, but it slightly affects the frequencies feature of the signal.

Cross-talk

Crosstalk noise occurs when the EMG signal, acquired through electrodes over a specific muscle, gets interfered with other signals coming from muscles located nearby. This mix of signals from different muscles can cause misinterpretation of the information. Even though this noise depends especially on physiological characteristics of the muscle, it can be minimized by carefully choosing the electrode size, position and inter-electrode distances.

Internal noise

Another noise component is the internal noise that affects the quality of the EMG due to biochemical and physiological factors, such as the number of muscles fibers per unit, the anatomy, the depth, the location of active fibers and the amount of tissue between contracting muscles and electrodes. The effects of internal noise, like the electrical activity of the heart, known as electrocardiogram (ECG) artefacts, can be partially reduced by applying some high-pass spatial filters.

Therefore, this chapter presented background information about the physiology of the muscle, focusing on the skeletal muscle. A detailed description of the internal muscle activity is provided in order to understand the contraction process. An explanation of the fatigue process, and the relative variable that could be used for evaluate muscle fatigue is given. Moreover, the EMG technique is presented, focusing on the parameter to be taken into account during an acquisition process. Finally, all kinds of noise that could be found within EMG signals are analyzed. This information, together with the presentation of the experimental platform provided by the second chapter, is useful to understand the strategies adopted during data acquisition and processing, which will be presented in the third chapter.

Chapter 2

Experimental Platform

The European BioMot project [39] focused on the development of a full lower-limb exoskeleton for gait rehabilitation [40], [41], and for assisting people suffering musculoskeletal impairments. The exoskeleton used in the project consists of three joints that make use of a new generation of Variable Stiffness Actuators (VSA) [42], [44]. Each joint is actuated by the novel spindle-driven joint-specific Mechanically Adjustable Compliance and Controllable Equilibrium Position Actuator (MACCEPA)[43], which is more efficient than position controlled stiff actuators thanks to its linear angle-torque characteristic and the decoupling of the control for the joint compliance and the equilibrium position [44]. For this study, only one single joint of the exoskeleton was used, that is the Motorized Ankle Foot Orthosis. The overall system architecture is depicted in Figure 2.1. In the ankle joint there is a custom designed and developed dsPIC-based driver board, namely a Secondary Processing Unit (SPU), which is responsible for the control of the actuated joint and for the sensor data acquisition, sending control output every 3 ms. Data from SPU are then gathered and packed by a custom designed ARM-based board that is responsible for the management of the CAN-bus communication towards the BeagleBone Black (BBB), a Central Processing Unit (CPU), at 100 ms intervals. This BBB board, running Ubuntu, interfaces the dsPIC-based driver board with MathWorks Simulink and MATLAB. In fact, a visual paradigm, which is a useful visual feedback for keeping high the user's attention during the experiment, was programmed in Simulink.

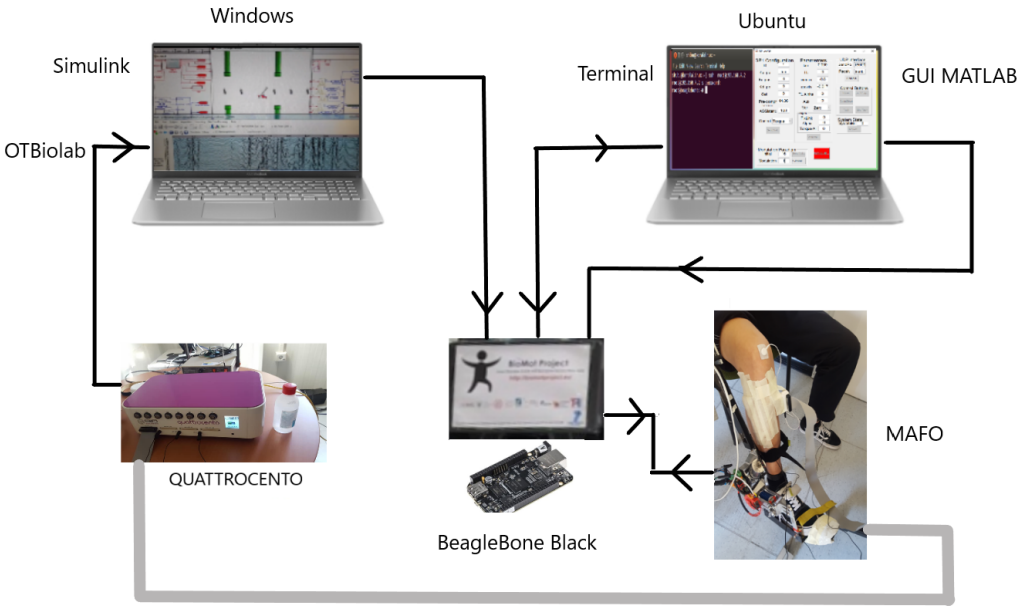

Figure 2.1. The overall system architecture.

Some control parameters for the robot could be changed on real time from a Graphic User Interface (GUI) designed in MATLAB. In addition, electromyographic signals were extracted by means of HD-sEMG technique; data were acquired with the QUATTROCENTO amplifier and were sent directly to OTBiolab software, where they have been recorded. Data processing was done in Matlab.

In the following sections we will first present the tibialis anterior and gastrocnemius medialis muscles, which have been evaluated in this work. Then, the design, the mechanical parts and the control strategy of the ankle actuator are explained. Finally, the software used for this work is described, focusing mainly on the innovative DEMUSE tool for the MUs decomposition, whose a brief user guide has been written to offer a fast guided approach to the tool.

2.1 Muscles of interest

This thesis investigates the major contributors to ankle movements in the sagittal plane, that is, ankle plantarflexor and dorsiflexor muscles. First the anatomy of the tibialis anterior is introduced, since it has been object of both studies; subsequently, the anatomy of the gastrocnemius medialis is described. In fact, before the electrodes placement, it is important to identify the right area of interest. In this work, SENIAM (Surface EMG for Non-Invasive Assessment of Muscles) recommendations [45] have been followed, asking to the subjects the execution of precise movements.

2.1.1 Tibialis Anterior

The tibialis anterior muscle, shown in Figure 2.2, is a lower leg muscle that lies in the anterior part of the leg and it is part of a group of extensor muscles. It runs medio-caudally from the lateral tibia, the interosseous membrane and the crural fascia. It is thick and fleshy above, and the fibers run vertically downward ending in a tendon.

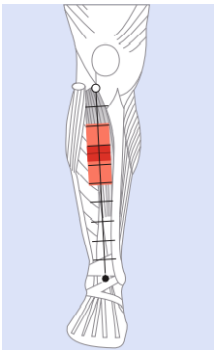

Figure 2.2. Tibialis anterior identification. Taken from [34]

It serves as the leading muscle for the neurovascular pathway running towards the ankle, which includes the deep fibular nerve and the anterior tibial artery and vein. Its main task is the dorsal extension of the upper ankle joint (dorsiflexion), but it is also useful in the assistance during the inversion of the foot.

2.1.2 Gastrocnemius Medialis

The gastrocnemius muscle, visible in Figure 2.3, is a lower leg muscle and, together with the soleus, it forms the calf in the posterior part of the leg. It is a biarticular muscle and it has two heads, called the medial head and the lateral head; these two heads are located from the medial and lateral condyles of the femur and have attachments from the knee joint capsule and from the oblique popliteal ligament.

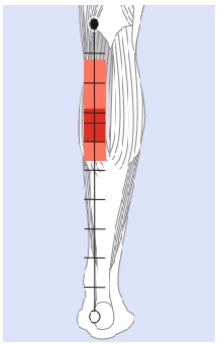

Figure 2.3. Gastrocnemius medialis identification. Taken from [34]

The fibers of the gastrocnemius run downward, where the two heads come together and insert into a membranous tendon, which fuses with the soleus tendon form the upper part of the calcaneal tendon. Its main function is the plantarflexion of the ankle, in addition to being a powerful knee flexor.

2.2 Motorized Ankle Foot Orthosis

In this subchapter, the mechanical designed of the ankle actuator, shown in Figure 2.4, is presented. The various components are described, starting from the variable stiffness actuator MACCEPA.

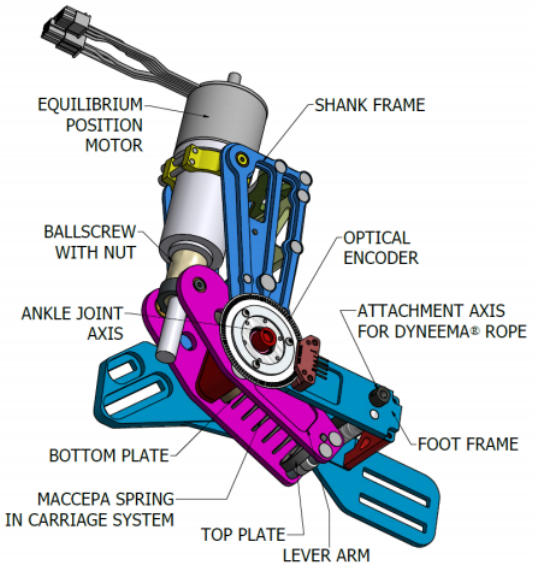

Figure 2.4. Mechanical design of the ankle actuator.

Then, the Motorized Ankle Foot Orthosis, built within the BioMot project, is examined in detail, concluding with the analysis of the implemented control strategy and the new control strategy proposed.

2.2.1 MACCEPA

MACCEPA is an innovative variable stiffness actuator that can be modelled as a torsion spring, allowing the independent control of the joint compliance and the equilibrium position. Different realizations of the MACCEPA have been developed because these rotational actuators are the most suitable type for many applications such as biped robots, prosthesis, stationary gait rehabilitation robots and exoskeletons.

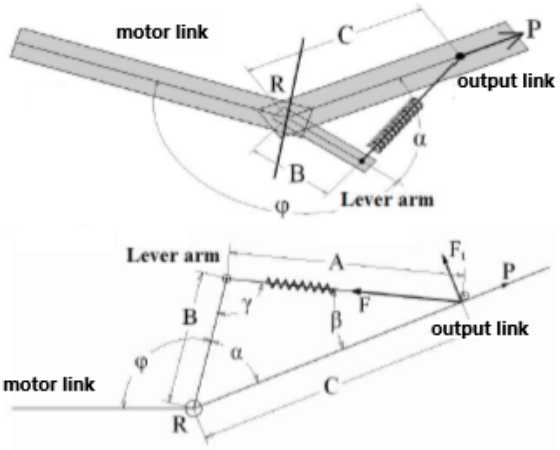

Figure 2.5. MACCEPA design.

In Figure 2.5 it is shown its scheme, where:

- A is the distance between the end of the lever arm, to which the spring is attached, and a fixed point on the output link,
- B is the length of lever arm, which sets the equilibrium position,
- R is the rotation point, around which the lever arm rotates,
- C is the distance between R and a fixed point on the output link,
- F is the force due to the extension of the spring,
- F_t is the orthogonal component of F that generates torque around R,
- k is the spring constant,
- α is the deflection angle between the lever arm and the output link,
- P is the extension of the spring caused by the pre-compression, which is equal to the total extension of the spring if α is zero,
- ϕ is the angle between the lever arm and the motor link, setting the equilibrium position
- τ is the produced torque on the output link.

As can be inferred from Figure 2.5, by applying some trigonometric formulas, the produced torque is obtained as:

$$\tau = k \cdot B \cdot C \cdot sin(\alpha) \cdot (1 + \frac{P - |C - B|}{\sqrt{B^2 + C^2 + 2 \cdot B \cdot C \cdot cos(\alpha)}}) \tag{2.1}$$

Now, by using small angle approximation, the equation can be linearized as follows:

$$\tau = k \cdot B \cdot C \cdot \alpha \cdot (1 + \frac{P - |C - B|}{\sqrt{B^2 + C^2}}) \tag{2.2}$$

that becomes

$$\tau = \alpha \cdot \frac{k \cdot B \cdot C}{|C - B|} - P \tag{2.3}$$

So, the linearized formula for the torque corresponds to a linear torsion spring:

$$\tau = \alpha \cdot \mu \cdot P \tag{2.4}$$

Thus, since μ and P are known a priori, the torque can be directly computed by the deflection angle α. In fact, the angle ϕ, and thus the equilibrium position, is set by a position controlled actuator, e.g servomotor. Therefore, if the output link and the lever arm are aligned, the angle α is zero and no torque is applied on the output link. Due to the alignment, the force exerted on the spring by a possible pre-load of the spring, has no effects. Instead, as soon as the equilibrium position of the lever arm is changed, by means of the ϕ set by the servomotor, a deflection angle α between the lever arm and the output link is generated. When α differs from zero, the force due to the elongation of the spring will generate a torque τ, according to the formula (2.4), on the output link around the joint axis. This torque tends to line up the output link with the lever arm, so that the output link moves towards the new position where no torque will be exerted. In the MACCEPA this motion is

bidirectional, that means both positive and negative torques around the joint axis can be exerted.

2.2.2 Ankle actuator

As can be seen in Figure 2.6, the actuator is composed of the motor and the output link, a brushless motor-spindle combination with the ESCON Module 50/5 servo controller, one absolute and one optical encoder, the spring inside the lever arm and a worm-gear pre-compression mechanism with Dyneema rope. Motor and output links have connection points for the shank frame and the toe plate, respectively, and the actuator range of motion is limited by mechanical stops.

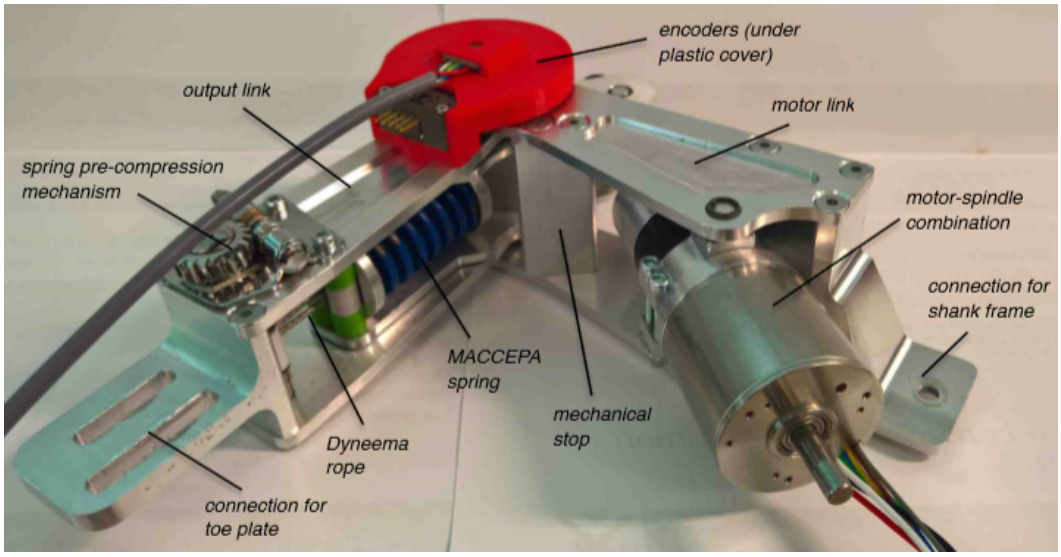

Figure 2.6. The mechanical ankle foot actuator used in this work.

The incremental optical encoder is used for measuring the biological angle, which is the angle between the motor and the output link, while the absolute magnetic encoder is used to compute the spring deflection angle α, that means the angle between the lever arm and the output link [39]. The spring pre-compression can be changed manually by means of a simple mechanism, robust and stable across different conditions, but it could be changed online by using additional motor. Finally, the spring was inserted inside the lever arm and, by performing a Finite Element Method (FEM) analysis, unnecessary material has been removed, producing a further

decrease in weight; in this way, the actuator is small and compact, while preserving its structural integrity. This actuator is attached at the top to a spring-steel frame plate whose profile is chosen so as to be stiff in the sagittal plane and flexible in the other two planes. This leg segment, as depicted in Figure 2.7, has two cuffs placed at the opposite side of the segment in the sagittal plane, one at the back and one at the front, to decrease the torque transmission losses and increase comfort.

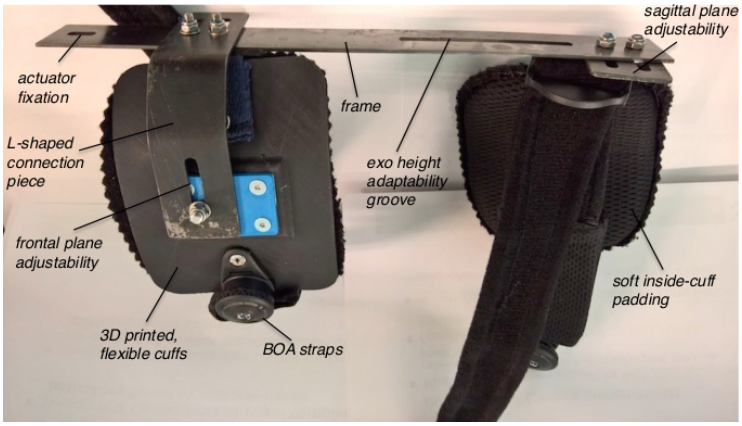

Figure 2.7. The spring-steel frame plate with the two cuffs.

These cuffs have an half-moon shape and a 3D printed flexible structure to make them easily adjustable to the user's leg shape. In order to fix them to the user's leg, an easy-to-use BOA closure system is employed. In this work the higher cuff has been removed for avoiding the contact with the HD-EMG matrix applied on the tibialis anterior, from which possible movement artifact could emerge. On the other site, at the bottom, the actuator is connected to a toe plate, which together with the heel plate form the footplate. These two parts of the footplate allows a perfect adaptation to the foot size of the user. Moreover, the right adjustability of these plates is made simple by using easily reachable same-size screws, in addition to a combination of easy-to-use Velcro and BOA straps, as shown in Figure 2.8.

Figure 2.8. On the left: the heel plate with the BOA straps. On the right: the toe plate with the Velcro strap.

2.2.3 Control strategy

BioMot strategy

In the Motorized Ankle Foot Orthosis a position-based torque control has been implemented. This control strategy tries to minimize the deflection angle α between the lever arm and the output link; this angle, as explained before, generates a torque, due to the spring elongation, in order to align the output link to the lever arm. Moreover, a tacit learning algorithm has been implemented in the adaptive control scheme used within the European project.

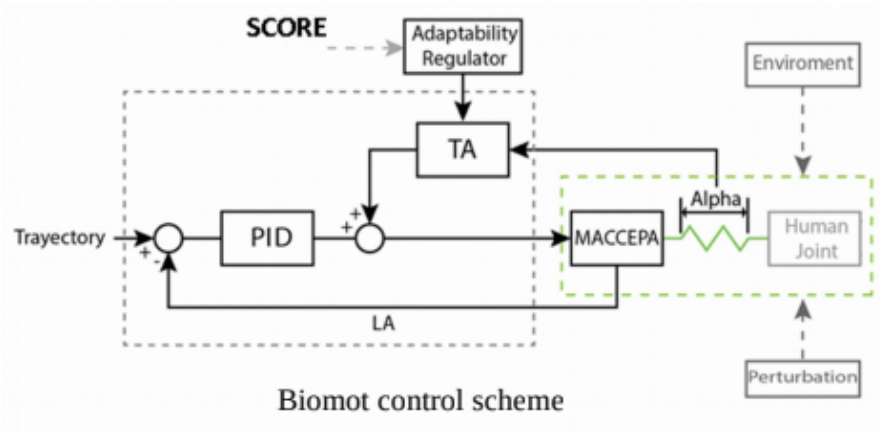

Figure 2.9. BioMot control strategy. Tacit adaptability constant changes according to the score of the user before modulating the controller output.

Tacit learning [46] is an unsupervised learning algorithm that, based on the principle of biological control, allows to create the appropriate behaviours in response to the interaction with the environment [47]. In fact, the primitive behaviours that are composed of the reflexive actions to deal with the environmental inputs are tuned to sophisticated behaviours in order to cope with environment changes [48], [49]. In the BioMot project, an adaptive control strategy was implemented. So, the user had to follow a given reference trajectory while the robot applied some perturbation chosen according to a specific rehabilitation purpose. In this case, if the user was not able to follow the trajectory, producing a bad score during the game, the robot decreased instantaneously the torque exerted, by means the Tacit Adaptability constant (TAc). In this way, the torque profile applied by the robot was automatically adapted to the user's capabilities. As can be seen in Figure 2.9, a Tacit Adaptability module has been added to the PID controller [50], [51]. This module consisted of an integral gain, called Tacit Adaptability constant (TAc) that relied on the instantaneous score of the user during an exercise. It worked in this way: if the user was not able to catch a bottle, which was used to visualize the desired trajectory on the screen, due to the great force exerted by the robot in the form of perturbation, the score decreased and the TA value increased. On the other hand, if the user was able to face perfectly with the robot perturbation catching all the bottles, which means following accurately the trajectory, the score, automatically computed, increased, and thus the TA resulted in a low value. Therefore, the score was inversely proportional to the Tacit Adaptability constant and it was computed on real time within the exercise. So, an high TAc modulated the force of the robot by making it lower, and thus more compliant to user's movement, while if the TAc constant decreased, the robot force applied against the user increased, resulting in a stiff behaviour. Finally, if the Tacit constant was zero, due to a perfect score (100%), the output of the controller was not modulate, and it worked as a normal torque control.

Proposed strategy

The idea behind this work springs from the desire to improve this control strategy by means of a new variable that was strongly correlated with the subject status. In fact, a score computed according to the quality of the exercise does not take into account the physiological condition of the patient. For example, if patients with musculoskeletal injuries or disorders are involved, large errors may be dangerous or undesirable; for this reason, it could be relevant to consider possible physiological changes in order to make the rehabilitation safer and more reliable. Furthermore, a robotic guidance could provide allowed or controlled movements for ensuring the right motor control learning. The conduction velocity was selected as indicator of muscle fatigue. Due to the large time requirements for the MU decomposition process, the CVs were computed offline and this control strategy could not be implemented.

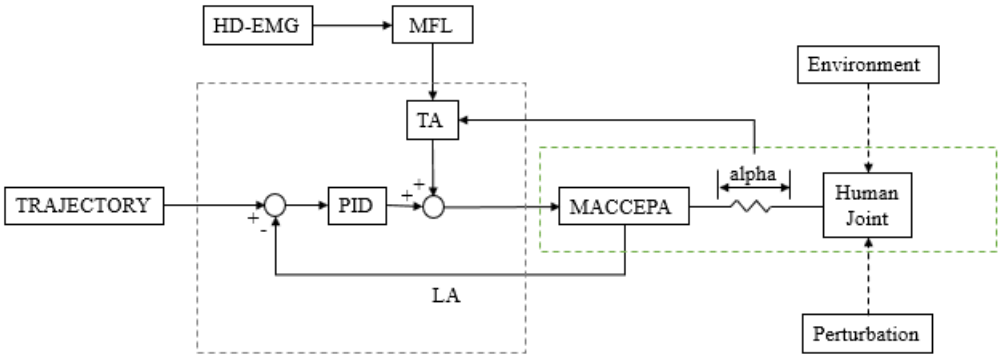

Figure 2.10. Proposed control strategy. Tacit Adaptability is informed of the Muscle Fatigue Level before modulating the controller output.

The proposed control strategy should automatically adapt the compliance of the wearable robot to the user's movement capabilities based on the Muscle Fatigue Level (MFL), which can be extracted from the HD-EMG by means of the muscle conduction velocity. As shown in Figure 2.10, the output of the torque PID controller should be modulated via the TA informed by MFL: it means that as soon as a CV variation is detected, a Muscle Fatigue Level is computed and the tacit adaptability constant changes, and thus it is modulate also the compliance of the torque control. So, when the exercise starts, the muscle fatigue level should be approximately zero,

and the same the TAc, being proportional to the MFL; thus, the controller act as a normal torque controller, applying the maximum level of force chosen for the specific user. As soon as the muscle starts to fatigue, the MFL increases, going to inform the TAc, which increases in turn and reduce the robot force. In the same way, when the muscle recovering is under way, the muscle fatigue level decreases, informing the TAc to reduce, so that the force output of controller will starts to come back to its original value. In this way the controller will change the compliance online based on physiological patients' features, trying to accelerate the rehabilitation process and at the same time avoiding the risk of bringing further damages to the injured muscle. Hence, during the rehabilitation exercise, which consists in following a given reference trajectory, the robot should apply some perturbation to the user according to definite torque profiles, in order to induce him making some specific movements, e.g. plantarflexion or dorsiflexion. As described, the value of this force should be modified along with the patient's level of muscle fatigue via the TAc, avoiding to ask the subject a huge muscle effort that could damage the fatigued muscle. This muscle fatigue level could be extracted from the conduction velocity of the nerve impulses; in fact, several studies have shown that muscle fiber conduction velocity decreases in presence of fatigue, bringing to a muscle strength reduction. Therefore, muscle fatigue could be a good parameter for modulating the output of the controller, so that the wearable robot will not force the user to overcome his physiological limits at each time instant. The control output is given by the equation:

$$\tau = K_p \cdot e(t) + K_i \int_0^t e(t)dt + K_d \frac{de(t)}{dt} + K_{TA} \cdot int\_lv \tag{2.5}$$

where τ is the torque generated, int_lv is the interaction level as a function of the deflection angle, K_p, K_i,K_d are the proportional, integral and derivative gain constants, respectively, K_{TA} is the TA constant gain, funtion of MFL level, and $e(t)$ is the error generated by the deflection angle, given by:

$$e(t) = \alpha_d - \alpha \tag{2.6}$$

This error, as clarified before, reflects the torque error, so that it has been possible to implement a torque control, starting from angular positions of the ankle orthosis joints. So, the maximum value of K_{TA}, which would represent an high muscle fatigue level, will lead to a zero-torque control, while the minimum value of K_{TA} that would correspond to a zero muscle fatigue level, will lead to a regular torque control; all the values of K_{TA} between the maximum and the minimum values, would changes the torque control accordingly.

2.3 EMG signal amplifier and electrodes

For data acquisition, the QUATTROCENTO multichannel amplifier for bioelectrical signals has been used. It is a research instrument designed for clinical research developed by OTBiolettronica in Turin [52].

Figure 2.11. QUATTROCENTO multichannel amplifier for bioelectrical signal acquisition.

The system amplifies, filters and digitally converts the signals; then, it transfers them to a PC, via an ethernet interface, for real-time visualization and storage, through a freeware software called OT BioLab. Quattrocento is a modular system that can acquire up to 384 bioelectrical signals, plus 16 auxiliary inputs (from here the name "quattrocento", since it potentially can acquire four hundred channels). In this work, a multiple input of 64 channels plus an auxiliary input connected to the robot has been used.

Figure 2.12. Electrode matrix ELSCH064NM2 with 64 electrodes of 8mm and its ashesive foam.

A semi reusable 64-channel matrix (ELSCH064NM2) with its adhesive foam, showed in Figure 2.12, have been used. In this matrix, channels are not ordered, and the inter-electrode distance is of 8mm.

2.3.1 OTBiolab software

OT BioLab is an acquisition and processing tool developed by OT Bioelettronica. According to the user choice, it is able to record up to four hundred channels. After connecting the QUATTROCENTO to the laptop, when the program starts, it is a good practice to modify in the tools options the number of channels to be acquired and the specific sampling frequency to be used. Then, in the setup editor (Figure 2.13), it is possible to select the specific sensor used, the adapter, the muscle and the side of interest. Once finished the setup, the user can press the visualization button, defined by the upper-left blue arrow, and the signals are displayed; here there is the possibility to define the time-scale, to zoom in or out on the signal, to define a specific time range of acquisition and finally, the signal acquisition can be started by pressing the record button [53].

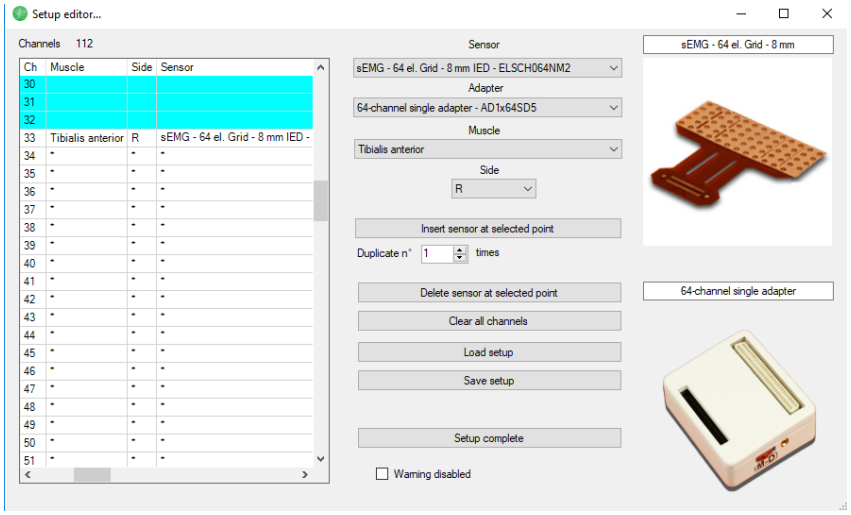

Figure 2.13. Setup editor of the Biolab software.

2.4 DEMUSE tool

DEMUSE is a commercial tool [54] widely used in the research for the visualization and decomposition of multichannel surface electromyograms by using the gradient Convolution Kernel Compensation (gCKC) technique [30]. It runs on Matlab and thanks to this software, it is possible to:

- load and visualize the multichannel surface electromyograms;
- decompose the EMG signals into contributions of individual motor units (MUs);
- display graphs of decomposition results, including plots of the MU discharge patterns, instantaneous discharge rate, motor unit action potentials (MUAPs) and their 3D animations;
- compare the original surface EMG signals to the reconstructed motor unit action potential trains (MUAPTs);
- save the decomposition results in Matlab files.

Moreover, every plot is displayed as a regular Matlab figure so that the user can freely manipulate it with the standard Matlab graphic tools. As showed in the

Figure 2.14, DEMUSE tool is the last layer of a three-tier system architecture. The first two layers identify the electromyographic signal amplifier (QUATTROCENTO) and the surface EMG acquisition software (OTB), explained in the previous sections, while DEMUSE represents the third layer, used for the decomposition of signals.

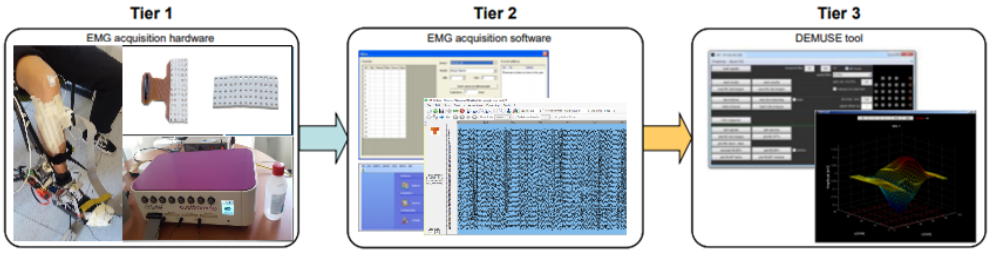

Figure 2.14. Three-tier system architecture. First layer: acquisition system preparation. Second layer: EMG data acquisition with OTBiolab software. Third layer: data processin with the DEMUSE launched in Matlab.

Once installed, when it is running on Matlab, a DEMUSE tool window appears containing four frames, whose it is possible select command for:

- loading data, band-pass filtering, visualization of the acquired surface EMG signals, and saving or reloading the decomposition results;
- decomposition option for the loaded EMG signals and manual inspection of decomposition results;
- graphical plots and animations of the decomposition results;
- selection of channels, rows and columns, in the matrix of HD-sEMG electrodes.

In the next subparagraph each step and component of the tool is fully described in order to create a fast guide for inexperienced user that want to approach the tool for the first time. The complete user manual of the DEMUSE is available online [55].

2.4.1 Description of DEMUSE tool usage

The first step is to download the signals by selecting the EMG file extensions in the Properties menu. DEMUSE tool supports arbitrary configurations and numbers of surface electrodes and it stores the information about the acquisition modalities in Matlab files called readers; at this point, DEMUSE tool prompts for the selection of a proper reader for EMG files. In this work, a simple CKCreader has been modified; since the electrode matrix used has not ordered channels, it has been implemented a channel re-mapping from the signal acquired with the OTB software. Here, it is important to define correctly some parameters like the sampling frequency, the dimensions of the acquisition system, the electrode configurations and the inter-electrode distance.

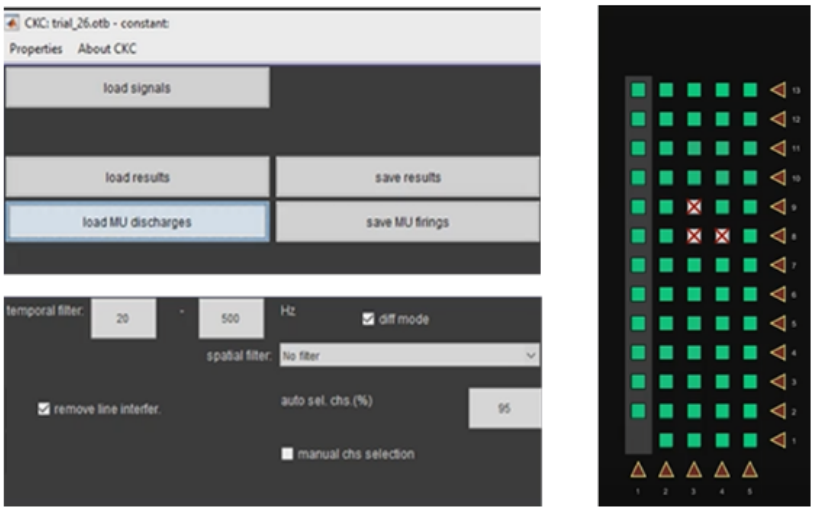

Figure 2.15. Saving, loading and filtering options in the first frame.

In the first frame, illustrated in Figure 2.15, in addition to the saving and loading buttons, the user is allowed to select some options. In the first two boxes, the user can choose the cut frequency of a 2nd order Butterworth band-pass filters for filtering the signals to be loaded. Moreover, for an experienced user, the high-pass and low-pass filters can be freely modified in the Matlab scripts. Then, there is the option to select the diff. mode box in order to activate the time differentiator, a simple high-pass filter which suppresses small MUAPs and enhances the discrimination of MUAPs

from different motor units. This box is recommended to be selected when the number of expected MUs in the EMG signals is high. DEMUSE tool automatically removes the line interference, but it can be avoided deselecting the remove line interference box. Additionally, it tests the acquired EMG channels for presence of movement artefacts and bad skin-electrode contacts. Hence, percentage of the EMG channels to be included into the decomposition can be specified explicitly by changing the value of auto sel. chs. textbox. The default value is 95%, which means that 5% of the channels with the lowest estimated signal quality will be discarded by the gCKC decomposition method. After selecting the desired options, the signals can be loaded; here a window pop-up allows the user to select the preferred CKCreader according to the EMG acquisition parameters. As the loading is complete, an electrode matrix will appear in the right frame, the Channel Selection Frame, which displays the number of acquired EMG channels and their relative spatial configuration. Some bad channels with a low quality are automatically marked with a red cross over the grey rectangle representing the electrodes; nevertheless, in this panel, the user is allowed to click on some specific electrodes in order to discard them or restore them from the analysis and visualization plots.

Figure 2.16. Decomposition options in the second frame.

In the second frame, which can be seen Figure 2.16, the user can start the decomposition process, by properly choosing the epoch offset, the length of the signal, and the number of decompositions run of the tool. Here it is possible to select the decomposition sections box, allowing to slide the epoch length window, which has to be decomposed, over the entire signal; otherwise, after a first decomposition over just one single epoch length, the user could change the offset and press the redecompose button, keeping the already identified MU discharge patterns and

adding them to those reconstructed in the new decomposition run. Besides, the EMG signals can also be decomposed in a batch mode, by clicking batch decompose button; in this way, the Reader Dialog Window opens offering the selection of CKC readers. After selecting the reader, the standard dialog box for selecting directory opens; once it is chosen the directory containing the signals to be decomposes, by pressing the ok button the decomposition process starts. All the signals in the selected directory will be sequentially loaded into the DEMUSE tool and processed. For the decomposition, the gradient Convolution Kernel Compensation (gCKC) decomposition technique, fully developed by Ales Holobar is used. Due to the high memory consumption of gradient CKC method and the large number of acquired surface EMG channels, the length of decomposition interval should generally be limited up to about one minute, depending on the available memory, while longer signals should be divided into 20-40s long epochs which should be decomposed independently. Then, the results can be fully analysed by clicking on the CKC inspector button.

Figure 2.17. Visualization options in the third frame.

Finally, the third frame, shown in Figure 2.17, contains all the buttons for the plots: the EMG signals (Figure 2.18) or their spectrum, the MU firings (Figure 2.19), the MU pulse train, the MU firing rates, the MUAPs of single MUs (Figure 2.20), the MUAP trains and the MUAP residual. All the plots are referred to the interval of the epoch length selected in the previous frame; furthermore, it is also possible to see the animation of the MUAP behaviour in that time interval. In addition, there is the option of sorting the MU with respect to the number of their discharges, the recruitment order or with respect to their identification accuracy as assessed by Pulse Noise Ratio (PNR) metric [56]. Currently selected MU to be investigated can

be moved upwards and downwards by pressing the MU up and MU down buttons, while those having bad quality or empty can be delete through delete MU and delete empty MUs, respectively.

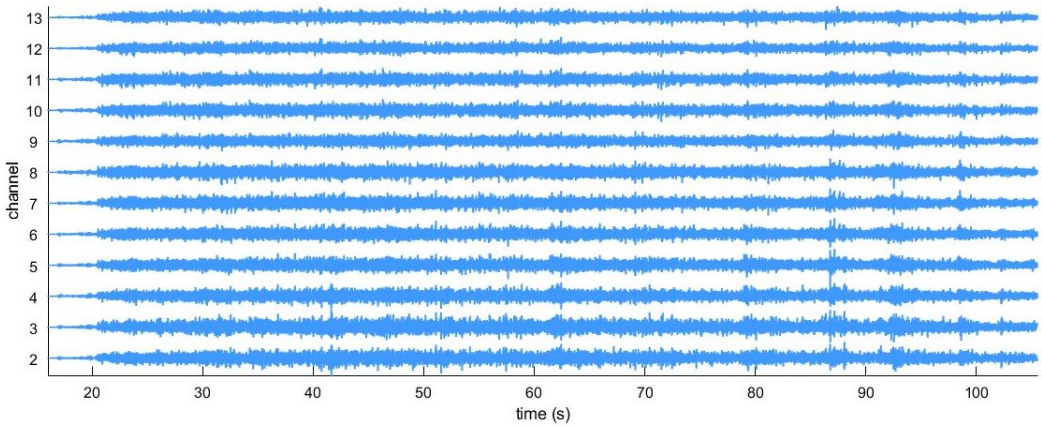

Figure 2.18. Plot of EMG signals acquired during long lasting contraction in the test at 80% (see chapter 4.2.1, subject 1). The last column of the electrode matrix is shown, where the first electrode was empty.

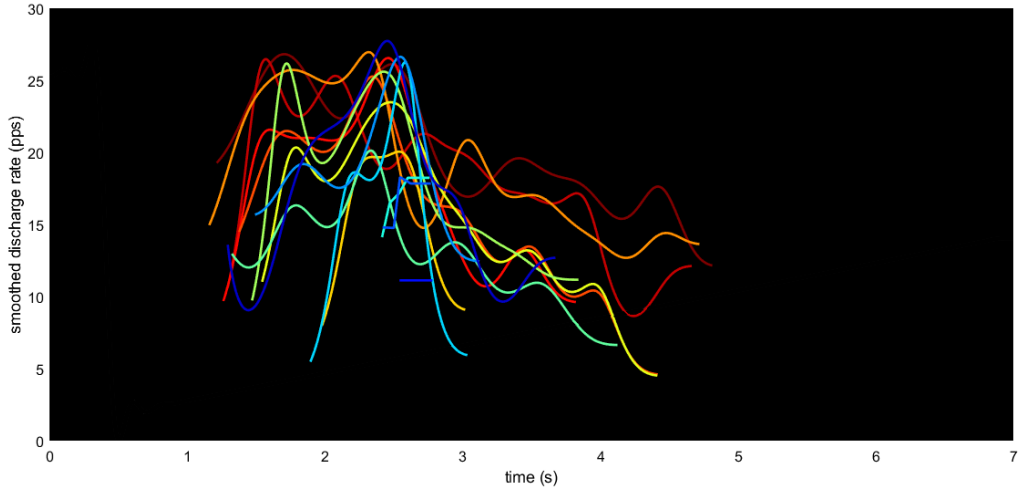

Figure 2.19. Plot of the 1^{st} MU firing rate in the first time interval during repetitive muscle contractions in the test at 80% (see chapter 4.2.2, subject 1).

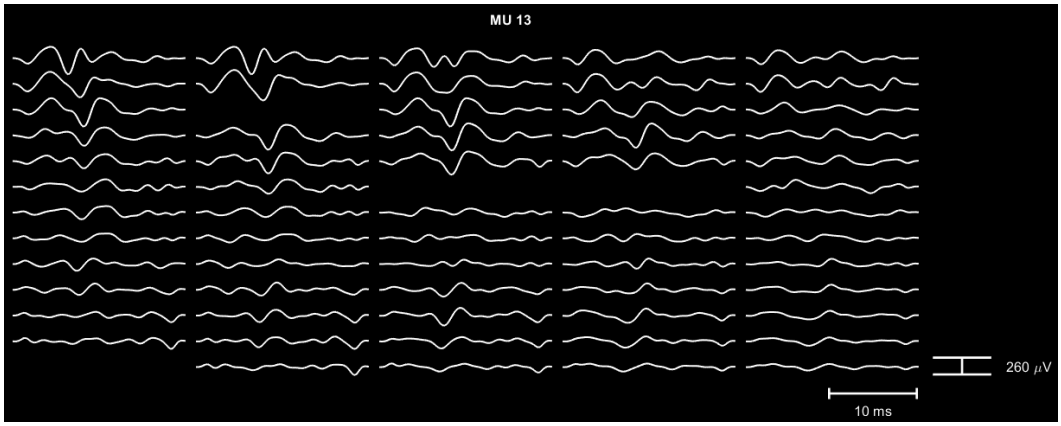

Figure 2.20. Plot of MUAPs of the 13^{th} MU in the first time interval during repetitive muscle contractions in the test at 80% (see chapter 4.2.2, subject 1).

CKC Inspector

The CKC inspector allows editing the raw outputs of the gradient CKC algorithm. It consists of three panels, which are from top to bottom:

- MUAP panel, which displays the multi-channel MUAP of the selected MU,
- IDR panel, which displays the instantaneous discharge rate (IDR),
- IPT panel, which shows the innervation pulse train (IPT).

In the first panel MUAP shapes for each channel are represented, excluding discarded channels. Furthermore, it is possible to see the number of firings and the PNR metric of each single MU; this PNR metric enables automatic assessment of accuracy in motor unit identification. In fact, with respect to other state-of-the art metrics in the field of EMG decomposition, this particular metric does not rely on regularity of MU discharge pattern. For this reason, it is considered a strong candidate for evaluating the quality of surface EMG decomposition in case of various diseases, such as pathological tremor, for which it is not always possible to guarantee the regularity of motor unit discharge patterns. Besides, PNR reflects the sensitivity and false alarm; in order to be accurate, it should be computed with at least more than 30 MU discharges and it should have a value greater than 30 dB: the greater the number of MU discharges, the more accurate the PNR metric.

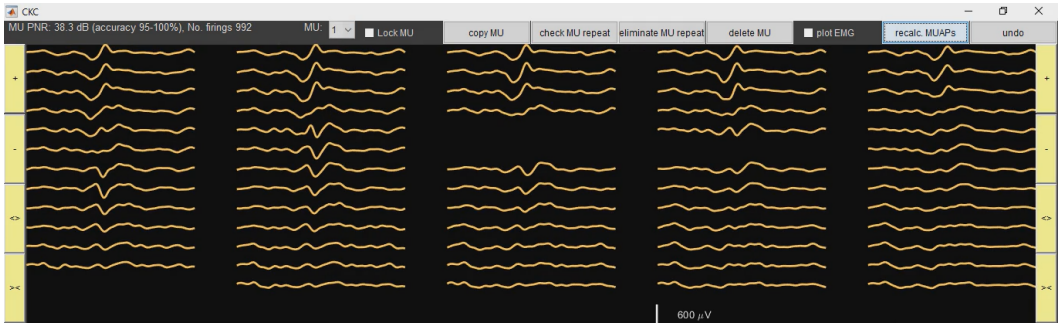

Figure 2.21. First panel of the CKCinspector.

In addition, there is the possibility of performing some actions on the selected motor unit, like copying it, deleting it, checking its repetition among the others or eliminating it. As can be seen in Figure 2.22, in the central panel, the instantaneous discharge rate is displayed. Moreover, a thin grey line is displayed, which represent the reference force of the reference signal, as determined by ref_signal in the CKC reader.

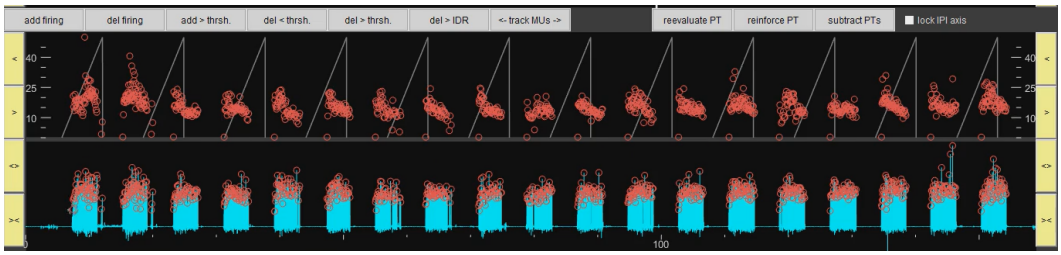

Figure 2.22. Central and last panels of the CKCinspector.

In the last panel, the train of MU discharge times, as estimated by the gCKC decomposition technique, are displayed. In both panels, the vertical axis denotes the instantaneous discharge rate in pulses-per-seconds (pps), while the horizontal axis denotes the time in seconds. On the top of the central panel there are grey buttons that allow to perform actions inside the plots, while on both sides of the panels there are yellow buttons with arrows in order to move along the signal, zoom in or zoom out, respectively. By using the first five grey buttons, it is possible to add and delete single firings or firings above or below a threshold, according to the button name, on the IPT panel. Thanks to the $del > IDR$ button, instead, it is possible to delete

firings above the chosen threshold in the IDP panel. The track MUs button allow to track over the entire signal the MUs identified on a portion of the signal. Thus, after zooming in the time interval with the identified MU discharge pattern, by clicking on this button, the algorithm iteratively identifies the MU discharges on the entire time support of the signal. In each iteration step, the algorithm searches for the discharges of all the identified MUs on the displayed time interval. The tracking is performed by automatically moving forward and backward from the current time interval for half of its length until the end or the beginning of the EMG signal is reached. This procedure is applied to all motor units, so it is important that each MU is active in the time interval chosen. As a rule of thumb, the selected time interval should be at least 20 seconds long; furthermore, the MUs should be active for at least 10 seconds, otherwise MUs will be tracked with low accuracy or even not tracked at all. and the quality of the output depends on the interval length: more can take several minutes. Finally, with the last three buttons, there is the possibility to improve the decomposition results. After zooming on a specific time interval the reinforce PT button executes one gCKC iteration recalculating the MU firings without altering the MU firing positions; on the contrary, reevaluate PTs button executes one gCKC iteration recomputing the MU firings and locally aligning them with the positions of new the maximums in estimated pulse train. The subtract PTs button, instead, can be used for subtracting pulse train of other motor units, being useful when weak MU pulse trains are merged with stronger MU pulse trains that have similar MUAP shape.

In this Chapters the experimental platform used for the two studies is presented. First, the muscles involved in the experiments are described. Then, the MAFO is illustrated, focusing on the innovative technology of the actuator. Here, a description of the implemented control strategy implemented and the proposed control strategy are provided. The High-Density surface EMG and the OTBiolab software for data acquisition is shown afterward. Finally, the DEMUSE tool, used for the MUs decomposition is explained.

Chapter 3

Methods and Materials

In this chapter two different studies are presented. The purpose is to find a good indicator of muscle fatigue that could be used within the tacit adaptability module for improving the existing controller. The first study focuses on muscle co-activation; the experimental setup and protocol will be explained providing the implementation of different co-contraction indexes. The second study concentrates on the computation of the conduction velocity. The acquisition process will be explained and the algorithm implemented for data processing will be deeply analyzed. The overview of the studies is depicted in Figure 3.1.

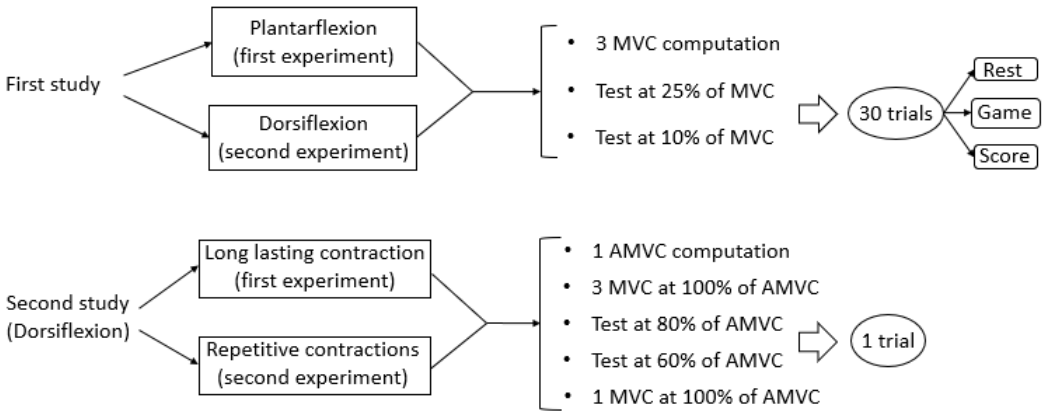

Figure 3.1. Overview of the experiments performed. Each arrow is used to explain more in detail each part of the study.

All the experiments have been performed by using the robotic platform previously presented in Chapter 2. All the data have been acquired with the EMG technique. Before going through the studies' presentation, the Approximated Maximum Voluntary Contraction value (AMVC) is introduced.

Approximated Maximum Voluntary Contraction value (AMVC)

Generally, due to the variability of the EMG signals, it is difficult to compare EMG data across different subjects, or even within different repetition of the same subject. One solution to overcome this problem is to normalize the EMG data to a reference value. As a rule of thumb, EMG data are expressed as percentage of the Maximum Voluntary Contraction (MVC) of the muscle of interest. This normalization is important because the raw EMG amplitude values vary so much across individuals; moreover, normalized EMG data allow to make comparison between different tasks, in addition to knowing how active muscles are with respect to their maximum capabilities. There exist several MVC methods in literature and some of them have become accepted as a standard thanks to their wide use [57]. In this work, since the robot force borne by the subjects was variable and a force sensor could not be used together with the robotic platform, there was the need of introducing a new variable. Thus, a new method was proposed, that is the Approximated Maximum Voluntary Contraction method (AMVC), in order to obtain a similar measure of the MVC for normalizing the data during the acquisition process. For computing the AMVC, each subject was asked to insert the leg inside the ankle orthosis and to perform a test exercise. Once a trigger was pressed, a straight line trajectory was visualized on a screen and the user was asked to follow the trajectory. Immediately, the robot started to apply a constant perturbation against the user. The force exerted by the robot was controlled via a modulation value, which can be changed online from the graphic user interface (GUI) in Matlab. The test started with a reference low value of the modulation paradigm, which means a low force exerted, and the user was asked to maintain the trajectory. Thus, if the subject was able to oppose the robot force and follow the trajectory, the modulation value was increased by one unit. This iterative process was continued until the user could not perform the

required movement and keep the trajectory anymore. At this point, the exercise was stopped and the modulation value was used as AMVC. Therefore, the robot force was expressed as a percentage of this value. This measure was adopted in the second study in order to choose the right modulation value for producing the same muscle contraction level across different subjects.

3.1 First study

The first attempt to find a measure of the muscle fatigue was to use a co-contraction index. A co-contraction index states the level of simultaneous activation of a muscle pair, typically known as agonist and antagonist muscles, that work in synergy for producing movements. This activity is considered as spontaneous collaboration between two muscles for stabilizing and preventing the joint from injuries. Moreover, it was found that co-contraction has also the potentiality of increasing the forces within the joint, so that it could be used in some control strategy for improving joint stability. On the other side, an excessive muscle co-activation might potentially lead to high risk of instability and it was associated to the progression of osteoarthritis [58]; furthermore, it was noted that strong muscle co-contraction increases the risk of excessive energy usage, resulting in muscle fatigue [59]. In the literature there are several ways of computing a co-contraction index relying on the surface EMG. After that a survey on the most used indexes has been taken, three different CIs were implemented in order to evaluate and compare their efficiency in terms of advantages and limitations and to investigate their potential to be an indicator of muscle fatigue.

3.1.1 Co-contraction Index computations

Although the quantification of co-contraction is difficult, electromyography (EMG) has become a common experimental tool to evaluate the magnitude of agonist and antagonistic muscle activity. It can be seen that the majority of the methods presented relied on surface EMG measurements. Usually, these signals are filtered according to a common data processing [60]: EMG raw data are full-wave rectified

and low-pass filtered. Then, the linear envelope of each muscle is extracted. Finally, EMG data are expressed as a percentage of the Maximum Voluntary Contraction (MVC). Besides these, for a better interpretation of muscle force, Knarr et al. [61] and Osu et al. [62] have proposed new CIs by using additional input parameters. The most used methods for computing the CI have been compared in the work of Kellis [63]. Two out of four were chosen, together with a third one, which has been proposed by Rudolph et al. [64]. The implementation of these indexes is the following:

- First, a modified version of the method by Falconer and Winter [65], used also by Iwamoto et al. [66], was implemented. Particularly, the following equation was used:

$$CI = \frac{2I_{antagon}}{I_{total}} \times 100 \tag{3.1}$$

where $I_{antagon}$ is the area of the total antagonistic activity. This was calculated using the following equation:

$$I_{antagon} = \int_{t_1}^{t_2} EMG_{m_1}(t)dt + \int_{t_2}^{t_3} EMG_{m_2}(t)dt \tag{3.2}$$

where t_1 to t_2 denote the period where the EMG of the first muscle m_1 is less than the other one (m_2), whereas t_2 to t_3 denotes the period where the m_2 is less than the m_1. I_{tot} is the integral of the sum of the muscles EMG during the whole task:

$$I_{total} = \int_{t_1}^{t_3} \left[EMG_{agon}(t) + EMG_{antagon}(t)\right] dt \tag{3.3}$$

where EMG_{agon} and $EMG_{antagon}$ indicate the sctivity of the agonist and antagonist muscle at time t.

- Second, the equation proposed by Frost et al. [67] and Unnithan et al. [68] was used. Here, the CI was computed by finding the overlap between the

agonist and antagonist curves and dividing the result by the total number of data points. So, a full overlap means that the CI point out a full co-activation of the muscles.

- Third, it was found in the literature the CI proposed by Rudolph et al.[64], used also in [69], which was calculated according to the equation:

$$CI = \sum_{i=1}^{N} \left[\left(\frac{LowerEMG_i}{HigherEMG_i} \right) \times (LowerEMG_i + HigherEMG_i) \right] /N \quad (3.4)$$

where N is the total number of time instants, while $LowerEMG_i$ and $HigherEMG_i$ represent the activation of the less active and more active muscle at the i-*th* time point, respectively.

3.1.2 Experimental setup and protocol

One healthy male subject (25 years old) volunteered for this study. The skin over the tibialis anterior and the gastrocnemius medialis was cleaned with alcohol before the electrode application. Two pairs of surface electrodes of 15x15 mm with 16-channel bipolar adapter Jack connector were applied on the muscles following the SENIAM reccomendation[45], as shown in Figure 3.2; the first two electrodes were placed over the tibialis anterior, while the other two were placed over the gastrocnemius medialis, both with a minimal inter-electrode distance ($< 30mm$). Moreover, two reference electrodes have been used, laying them on the ankle as suggested in [4]. Regarding the protocol, it was composed of two parts:

1. computing the MVC three times,
2. performing two tests, one at 10% and one at 25% of MVC,

The MVC for the gastrocnemius was recorded by asking the user to stand on his tiptoe with one leg, as in [70], while the MVC for the tibialis was computed by asking the user to oppose with all his/her strength to a high manual force pulling back his tiptoe, causing him to produce a dorsiflexion.

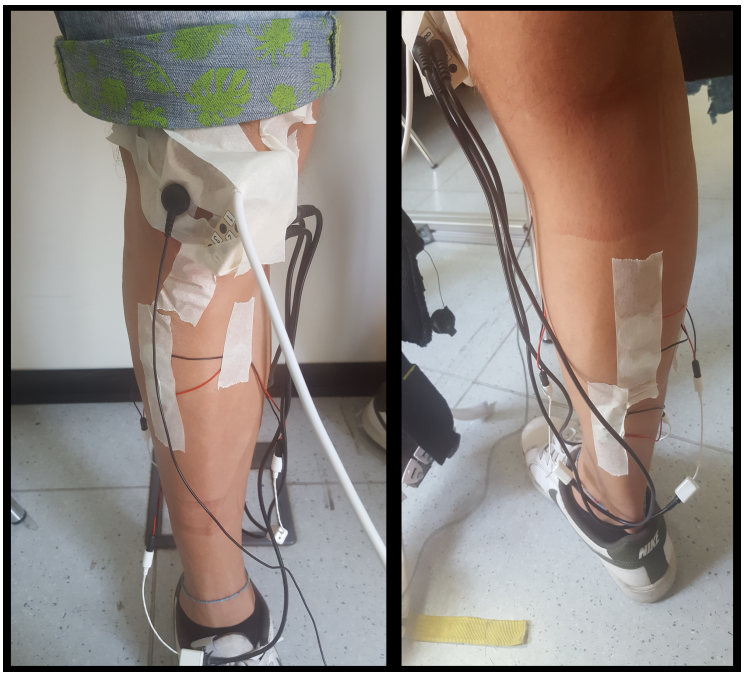

Figure 3.2. On the left the electrodes placed over the tibialis anterior and the connector are shown. On the right the electrode application over the gastrocnemius is shown.

Then, the subject was asked to put the leg inside the ankle orthosis and the straps were tightened so as to best suit the user's leg. At this point, before starting both tests, the equilibrium position ϕ of the robot, indicated by the lighting of a green light on the SPU, was manually set. Both tests of the experiments, exactly as in the BioMot project, consisted of thirty trials, each of which lasted around fifteen seconds. Every trial consisted of three parts: rest, game and score. The test started when a trigger button was pressed. During the game, which lasted exactly ten seconds, the user was asked to follow a straight line trajectory, trying to compensate the perturbation applied by the robot. In order to facilitate the task, the user was provided with a visual feedback on the screen. The angular position of the foot plate was visualized on the screen through a small red helicopter while the trajectory was identified with some bottles, like in Figure 3.3.

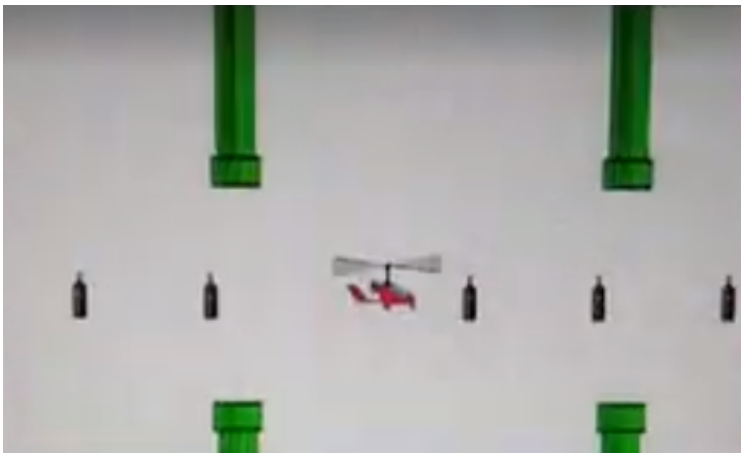

Figure 3.3. Visual feedback for the user. The red elicopter represents the foot angular position.

The torque patterns implemented in the controller are shown in Figure 3.4. The perturbation started increasing from 2 to 5.5 seconds and then decreasing from 5.5 to 8 seconds. In the first experiment, the robot generated a force upward, causing the user to contract the gastrocnemius, and thus producing a plantarflexion; in the second experiment, the robot generated a force downward, causing the user to counteract by contracting the tibialis anterior, and thus performing a dorsiflexion.

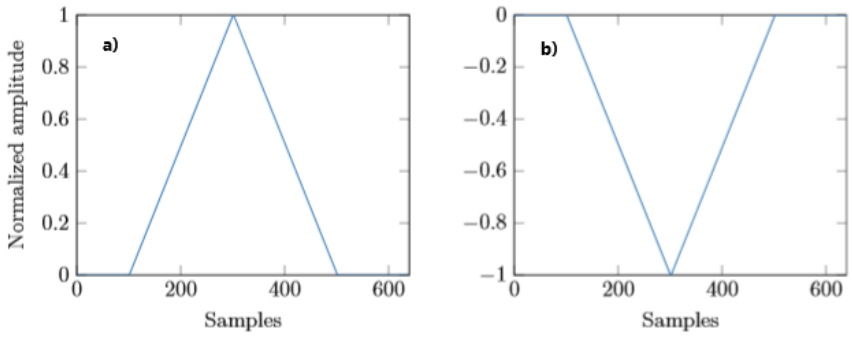

Figure 3.4. a) Torque pattern used for causing a plantarflexion; b) torque pattern for causing a dorsiflexion.

3.1.3 Data acquisition and processing

The EMG signals have been acquired in a bipolar configuration with OTBiolab at a sample frequency of 5120 Hertz. An auxiliary input was exploited for storing a trigger signal, which has been used to synchronize EMG signals with the data from the robot. Data from the orthosis, e.g. torque profile, user's trajectory, target path and trial's part, were recorded directly in the Matlab workspace at a sample frequency of 64 Hertz. All EMG data were converted in a *.mat* file and then processed in Matlab. The first step was to synchronize the EMG signals with the data obtained by the robot thanks to the trigger: all the EMG signals have been cut in order to start at the same time instant in which the trigger signal was encountered. Then, since the time frequency of the acquired robot data was less than that of the EMG signals, a resampling was performed. Subsequently, the EMG signals have been filtered by performing:

- band-pass filter at the cut-off frequencies of 10 and 500 Hz,
- full-wave rectification,
- liner envelope with a low-pass filter of 2 Hz, as in [60] .

The next step was to normalize the EMG signals, expressing them as a percentage of MVC; afterwards, the time interval corresponding to the game parts was extracted, excluding the rest and the score parts. At this point, each co-contraction index was computed in a time window of 50 ms, which moved along the entire signal with no overlap, obtaining the overall CI trend. The three co-contraction indexes performance will be examined and discussed in the next chapter.

3.2 Second study

In the second study, the analysis of muscle conduction velocity was performed. As explained in 1.3.4, several investigations have found that a decrease in the CV indicated the presence of muscle fatigue. Therefore, two exercise were proposed for causing fatigue, a Long Lasting Contraction (LLC) and a test with Repetitive Contractions (RCs). The signals were acquired through High Density surface EMG and the signals were decomposed in order to allow the analysis of CV behaviour even at motor units' level. MUCV, MFCV and other EMG descriptors were compared between two test level for one subject, and then between two subject at the same level. In addition an automatic way to choose the correct CV value from the electrode matrix was implemented and evaluated. Finally, the relation between conduction velocity and muscle fatigue is investigated, highlighting the possibility of use this variable inside a myoelectric-based control strategy.

3.2.1 Conduction velocity computation

The conduction velocity within a muscle can be measured via intramuscular or surface electrodes. Usually this variable is computed between two electrodes placed at a fixed distance along the muscle fiber, according to the formula:

$$cv = \frac{\Delta s}{\Delta t} \tag{3.5}$$

where Δs is the inter-electrode distance and Δt is the time delay of a signal reference point, e.g peak or zero crossing, between the two different location. Usually the inter-electrode distance is fixed and known, while the computation of the time delay is hard due to resolution time problems. In fact, the estimation of the time delay was addressed in the literature proposing different methods, like minimization of the mean squared error (MSE) in the frequency domain [71] or computing the delay from the phase difference between the Fourier transforms of the signals [72]. In this work, for addressing the problem of CV estimation, the fast and high-resolution algorithm proposed by Farina et al. in [27] was used with permission. This technique extends the modified beamforming method [73] and the maximum likelihood estimation

(MLE) [74] searching for the minimum of the mean square error by finding the zero of its first derivative through the iterative Newton method.

3.2.2 Experimental setup and protocol

Five healthy subjects (two males and three females), with a mean age of 24, participated in this study: the first exercise was performed by one subject, while the second exercise was performed by all the participants. The two experiments were performed in different days. The following procedure was utilized for each subject. The skin over the tibialis anterior was cleaned with alcohol before placing the electrodes. A conductive gel was applied over the electrode matrix, composed of 64 electrodes with an inter-electrode distance of $8mm$. The matrix was placed along the muscle fibers direction according to the SENIAM reccomendations [45], as shown in Figure 3.5, and a reference electrode was placed on the knee. All the electrodes was connected to the QUATTROCENTO through a 64-channel single adapter,

Figure 3.5. Adhesive foam of the electrode matrix applied over the tibialis anterior according to [45].

The electrode matrix was secured to the user's leg with scotch tape in order to avoid movement artifact during the exercises. Moreover an interference reduction circuitry, called Driven Right Leg (DRL), was used in order to remove the common mode interference on the patient body. To activate this circuitry, ground strips

were connected to points on the subject's body without myoelectric activity, e.g. wrist and ankle, as suggested in [75]; furthermore, to ensure a good electric contact with the user, the strips were wet with water. The experimental platform during an experiment is shown in Figure 3.6.

Figure 3.6. Experimental platform used during an experiment. Ground strips for the DRL are highlighted with red squares.

Therefore, the subject was asked to put the leg inside the ankle orthosis and the straps were tightened to best suit the user's leg.

Before starting, the AMVC value, which is equivalent to the maximum force of the robot that the user can oppose, was computed, as explained in detail at the beginning of chapter 3. At this point, prior to starting each part of the test, the setup editor in OTbiolab was properly set and the program was launched for the signals visualization; furthermore, the equilibrium position ϕ of the robot was manually positioned at zero, indicated by the lighting of a green light on the SPU. The protocol consisted of recording signals during the following activities:

- Three constant contraction at 100% of AMVC for the MVC computation,
- Two tests, one at 80% and one at 60% of AMVC,
- One constant contraction at 100% of AMVC for the MVC computation.

In the first experiment (2.1), the trial was carried out performing a long lasting contraction, while in the second experiment (2.2) the trial was done performing 19 repetitive contractions.

1) The constant isometric contraction at 100% of AMVC lasted about 7 seconds and it was recorded three times with an interval of 1 minute. In this part, as soon as the user pressed the trigger for starting this initial test, the force exerted downward by the robot immediately increased and remained constant until the end.

2.1) The subject was asked to complete the first trial at 80% of AMVC, take five minutes of rest and complete the same trial at 60% of AMVC. The trial consisted in following a straight line trajectory, while the robot exerted a constant force against the user in the downward direction, causing him to perform a dorsiflexion. The whole trial lasted about 150 seconds.

2.2) The subject was asked to complete the first trial at 80% of AMVC, take five minutes of rest and complete the same trial at 60% of AMVC. The trial consisted in following a straight line trajectory, visualized on the screen as before (see Figure 3.3), while the robot applied 19 perturbation in the downward direction, causing the user to contract the muscle. Each contraction lasted 5 seconds and was interspersed with 5 seconds of rest, where no force was applied by the robot. The whole trial lasted about 150 seconds. The torque profile implemented in the robot controller is shown in Figure 3.4 *(a)*, so as to induce the user to perform a dorsiflexion.

3) Another constant contraction at 100% of AMVC was recorded at the end of the experiment. This has been useful to investigate a change in the EMG descriptors between the beginning and the end of the experiment, ensuring the possibly characterized the presence of muscle fatigue.

3.2.3 Data acquisition and processing

The EMG signals have been acquired in a monopolar way as suggested in [4](p.338) at a sample frequency of 5120 Hertz. Once EMG signals have been recorded, they have been loaded on the DEMUSE for the decomposition. The high and low pass filters were left unchanged at their default values, 20 and 500 Hz respectively, and the Power Line Interference (PLI) was removed. Since the channels of the specific electrode matrix used in this work were not ordered during the acquisition, a channel remapping has been added to the code for loading the signal. After the loading was complete, the time interval of the first two contractions was identified through the EMG signals plot. Once this time interval of 20 seconds was specified, by adjusting the epoch length offset, the decomposition process through the gCKC method was launched, performing 50 decomposition runs. As soon as this process was finished, the offset was changed in order to select the epoch length comprising the last two out of nineteen contractions. The decomposition process was launched again, performing other 50 decomposition runs. In this way a lot of Motor Units were identified. At this step it has been necessary to use the *track MU* button, so that the algorithm identified the discharges of the same MU and merged them. Then the CKC inspector was closed, and the empty MU were deleted. Regarding the first experiment, only a 20 seconds window at the beginning of the contraction was decomposed before starting the tracking algorithm. Finally, the quality of the decomposition results were checked through the plot options and saved in a *.mat* file. These data were processed in Matlab modifying the algorithm developed by Ales Holobar with his kind permission. The structure of this algorithm is the same for both experiments; nevertheless, time interval for the CV computation are different for the two experiments. The signals acquired from the electrode matrix were loaded from the *.mat* file and filtered with a high-pass filter and a low-pass filter at cut-off frequencies

of 20 an 500 Hz, respectively. Besides, the differential signals between adjacent channels were computed; these signals have been used for computing the muscle fiber conduction velocity according to the equation 3.5. All the EMG descriptors were evaluated in a time window of 250 ms, as suggested in [76], which was slidden along the entire signal without overlap, obtaining the overall behaviours. In the second experiment, these variables have been computed sliding the time window during the contractions, while they have been set to zero during the 5 seconds of rest. For the analysis, 3 seconds of each contraction are analyzed, removing the disrupt parts of the signals, e.g. 1 second at the beginning and 1 second at the end of the contraction. First, the Muscle Fiber Conduction Velocity (MFCV) was computed using the Maximum Likelihood multiple-channel method proposed by Farina [27]. Then, a second estimate of the Muscle Fiber Conduction Velocity (MFCV2) was extracted from the differential signals as the ratio of inter-electrode distance and time delay, computed through the cross-correlation of signals; here, an upsampling with an interpolation factor of 10 was performed so as to increase the resolution of signals and to obtain a more accurate time delay. In addition, the Mean frequency (MNF), the Median Frequency (MDF) and the Root Mean Square (RMS) were also computed at global level. Finally the Motor Units Conduction Velocities (MUsCVs) were computed for each MU that presented a PNR greater than 30, which means an accuracy of 90-100%. For evaluating the CVs behaviour along the entire signals, two channels were manually selected. Moreover, an automatic way for selecting the channels at each time interval was implemented. This algorithm, based on the highest correlation value between the signals for selecting the CV, adopted a nearest neighbor strategy, so as to avoid abrupt changes in the conduction velocity.

In this Chapter the two studies are presented. It starts with the First study, where CIs have been computed in two different experiments. Then, the Second study is explained, showing the experiments from which the CV was computed.

Chapter 4

Results

4.1 First study

In the first study three co-contraction indexes were computed firstly during a plantaflexion and then during a dorsiflexion; both were done at two different levels of MVC. All the co-contraction indexes were normalized through the use of the MVC, which has been computed as the mean of three different MVC acquisitions. Only the results of the test at 25% of MVC will be presented and explained, since the test at 10% of MVC showed the same results but with smaller amplitudes. During the first exercise, the user was instructed to perform a plantarflexion. As can be seen in Figure 4.1, when the game started, the level of co-contraction between the agonist and antagonist muscle was greater than zero because both muscles were active, even if in a low percentage of their relative MVC. When the robot started to apply a force against the user, causing him to produce a plantarflexion and thus contracting the gastrocnemius, the amplitude of the GM signal increased while that of the TBA signal went to zero; this happens because during the contraction, the antagonist muscle (TBA) started to relax. This brought to a co-contraction index level around zero, which can be seen in the 3-8 seconds time interval. As soon as the robot finished exerting the force, the user stopped contracting the GM and, as can be noticed, there was a TBA activation to decelerate the foot ascent movement and preventing the subject from injuries. This behaviour has been found almost the same along all the 30 trials of the exercise.

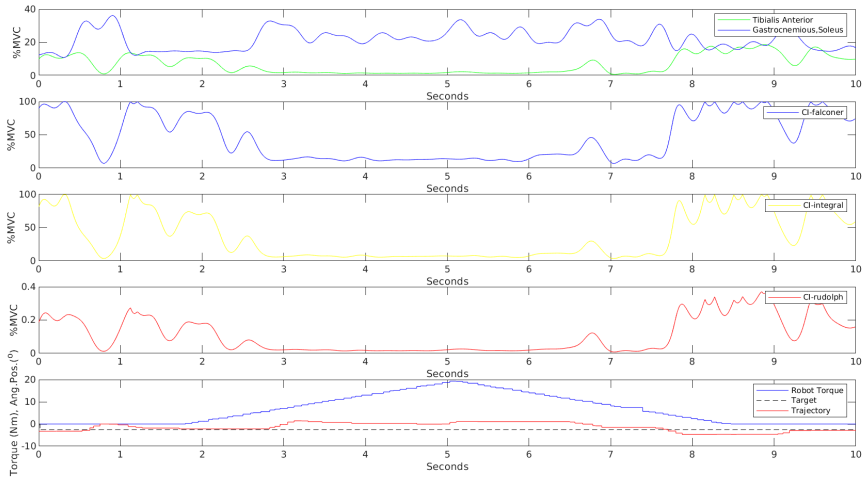

Figure 4.1. Representative timecourses of EMG indices during the exercise of plantarflexion (25% MVC) in Study 1. First subplot: tibialis and gastrocnemius EMG signal. Second subplot: CI computed according to [65]. Third subplot: CI computed as integral overlap of signals, used in [67] and [68]. Fourth subplot: CI computed according to [64]. Fifth subplot: robot torque exerted (Nm), target and trajectory player path (angular position).

While the first two indexes are almost perfectly equal, the third one, which is computed according to [64], is also normalized with respect to the total myoelectrical activity recorded. This takes into account the amount of the muscle activity used and, for this reason, the third CI results in a more precise value if compared with the other two indexes. Nevertheless, all of them present the same behaviour during each trial of the exercise. In this exercise, the indexes exhibited a constant pattern that could make it possible to recognize the GM activation with respect to the TBA activation. The same results have been obtained in the test of the plantarflexion at 10% of MVC, even though a further decrease of the third CI value has been encountered due to the less muscle amplitudes. Therefore, the co-contraction index could be used as a good indicator of muscle activation, but no realation was found with muscle fatigue. In fact, according to [77], muscle fatigue should produce an increase of the antagonist muscle activation, generating an higher CI different from zero even during the agonist contraction. Unfortunately, the contraction was too low to produce fatigue, so other experiments in this direction should be performed.

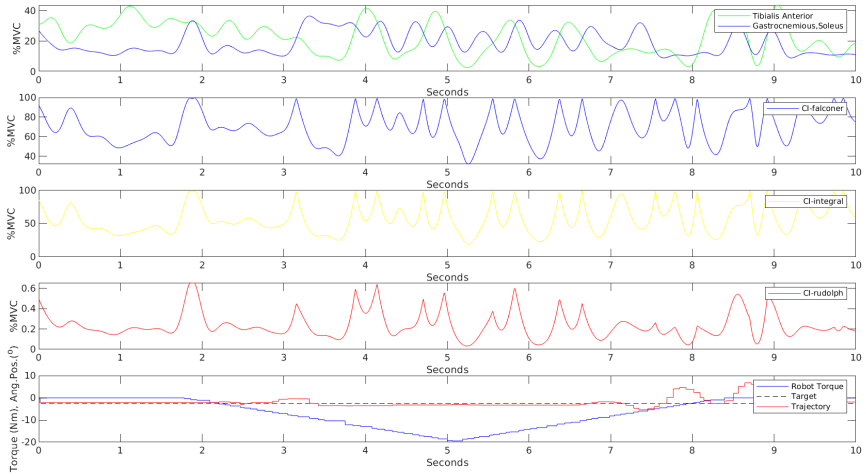

Figure 4.2. Representative timecourses of EMG indices during the exercise of dorsiflexion (25% MVC) in Study 1. First subplot: tibialis and gastrocnemius EMG signal. Second subplot: CI computed according to [65]. Third subplot: CI computed as integral overlap of signals [67] and [68]. Fourth subplot: CI computed according to [64]. Fifth subplot: robot torque exerted (Nm), target and trajectory player path (angular position).

Regarding to the data acquired in the other test, namely the dorsiflexion at 10% and 25% MVC, similar result were expected, but they were not verified. In fact, as can be seen in Figure 4.2, the CIs behaviour is oscillatory along the whole time interval. A possible explanation could reside in the fact that the MVC percentage of the TBA is too small with respect to that of the GM, creating this undesired behaviour. Another cause of this unstable behaviour could be an elevate presence of noise in the signals acquired, that made the CI analysis difficult. Even in this case, other experiments should be performed, in order to see if a CIs pattern can be encountered during cyclic isometric contractions of the TBA.

4.2 Second study

In the second study, the muscle fiber conduction velocity and motor units conduction velocities were computed. Moreover, other EMG descriptors were computed and evaluated in order to ensure the presence of muscle fatigue. In both experiments, the conduction velocities were computed between each pair of channels in the electrode matrix; so, starting from a 13x5 electrode matrix and computing the differential signals, a 11x5 CV matrix was computed. Moreover, each CV value was associated to a correlation value, which indicated the correlation between the two signals selected for the CV computation. The CV values considered are those derived from manually selected electrodes. The automatic algorithm for selecting the best channels is not presented, since it yielded results outside the plausible physiological range.

4.2.1 Long lasting contraction

The first experiment analyzed is the long lasting contraction, in which the robot exerted a constant force against the user, causing him to perform a dorsiflexion. For the following results, two single channels were manually selected, chosen according to the highest correlation value between signals.

Subject 1, Test 80% of AMVC

During the Long Lasting Contraction test at 80%, MFCV and MFCV2 values were computed and compared, showing a Pearson correlation coefficient $\rho = 0.9977$ and a p-value $p < 0.0001$, indicating that the upsampling method for the time delay gives similar result to the method developed by Farina [27]. This similarity was proved also for the test at 60%, where a coefficient $\rho = 0.9967$ and a p-value $p < 0.0001$ were found between MFCV and MFCV2. All the MFCV and MFCV2 values in the first test, computed every 250 ms, are depicted in Figure 4.3, where the general behaviour is provided by the cubic interpolation of the generated points. It can be noted that the MFCV, as well as MFCV2, decreased from 5.6 to 4.6 m/s during the whole exercise. This decrease in the CV is considered a myoelectric manifestation of muscle fatigue.

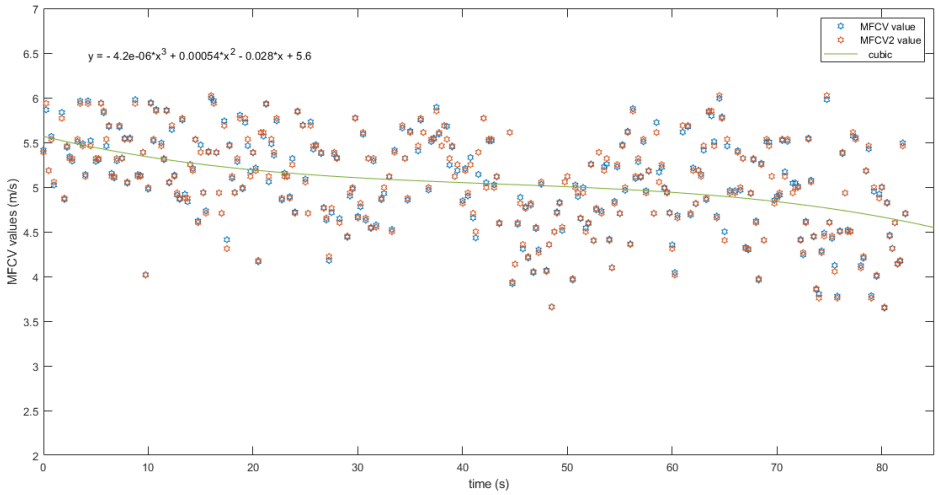

Figure 4.3. MFCV and MFCV2 in test at 80% of AMVC. Time evolution of the CVs during the long lasting dorsiflexion.

In order to ensure this result, two more EMG descriptors were computed, namely the RMS and MNF, that can be seen in Figure 4.4. The amplitude of the signal (RMS) tends to increase before going slightly down towards the end.

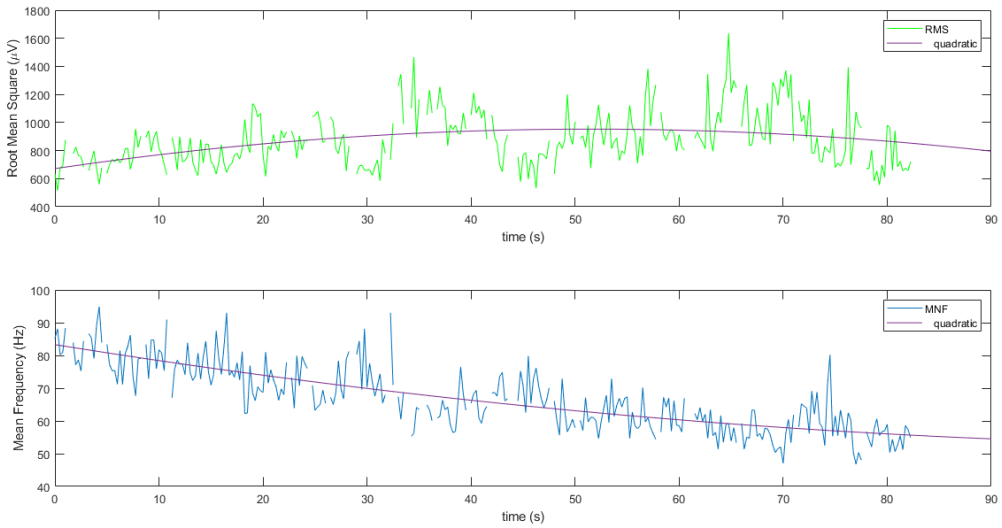

Figure 4.4. EMG descriptors in test at 80% of AMVC during the long lasting dorsiflexion of first subject. First subplot: RMS with quadratic interpolation. Second subplot: MNF with quadratic interpolation.

The frequency content of the signal (MNF), instead, is compressed, going linearly towards lower values. These results, according to [17], point out the presence of muscle fatigue. Then, all the MUs conduction velocities were extracted from the same electrodes. Each MU showed a fluctuating response during the whole exercise. This happens because each MU fires with a specific frequency, due to the refractory period where the MU cannot be excited. Thus, in order to keep the contraction and generate the same muscle force required by the user, other MUs are recruited and activated within the muscle. Therefore, a correlation coefficient was computed between each pair of motor units, but the results have no significant evidence. For this reason, a possible correlation between the MUs was not identified. Moreover, the mean and median of all the MUsCVs have been evaluated, once with respect to time, once with respect to the MU number. It was found, as shown in the table 4.1, that MFCV during the exercise has a correlation with the CV mean of all MUs (24 MUs in the first test), whose value is $\rho_1 = 0.6454$ with strong significant evidence $p < 0.0001$, while the correlation between the time evolution of MFCV and the time evolution of the CV median of all MUs is $\rho_2 = 0.6972$, again with strong significant evidence $p < 0.0001$.

Table 4.1. Correlation between MFCV and MUsCV for the two tests of the first subject. Here, ρ_1 is the correlation coefficient between the MFCV and the mean of all MUsCV, while ρ_2 is the correlation between MFCV and the median of all MUsCV.

AMVC	ρ_1	ρ_2
test 80%	0.64 ($p < 0.0001$)	0.69 ($p < 0.0001$)
test 60%	0.60 ($p < 0.0001$)	0.67 ($p < 0.0001$)

The means (and their standard deviations) of all CVs for each Motor Unit are shown in the first subplot of Figure 4.5. It can be noted that the last MUs present a very low mean. This happens because they are activated later during the exercise, so in many time instants their CV values are zero; instead, the first MUs, active from the beginning, have a normal CV mean with a great standard deviation, depending on the frequency at which they fired. In the second subplot, instead, it is represented

the evolution in time of the mean of MUsCVs at each time instant. Even here, the cubic interpolation of the points shows a decrease from 5.1 to 4.2 m/s, giving another proof of the muscle fatigue presence.

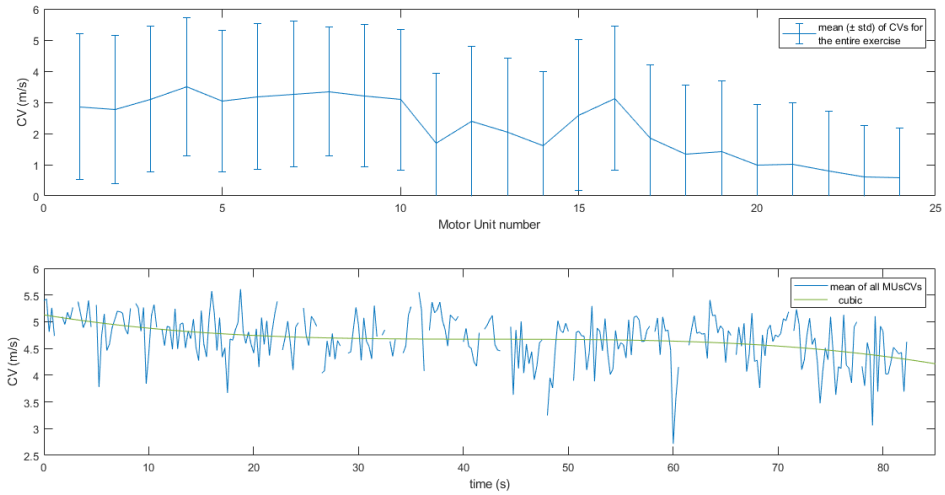

Figure 4.5. MUsCV in test at 80% of AMVC of the first subject. First subplot: mean of all CVs for each Motor Unit. Second subplot: time evolution of the mean of CV values derived from all MUs at each time instant, with cubic interpolation.

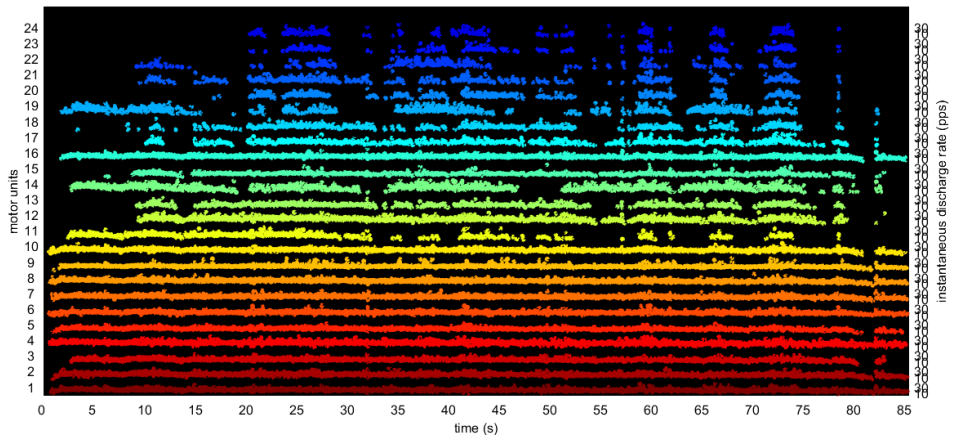

Figure 4.6. MUs firing in test at 80% of AMVC of the first subject.

Finally in Figure 4.6 it is possible to note the MUs firings along the whole exercise. As said before, some MUs have some "holes" because they are activated only in specific time intervals to support the previously active MUs.

Subject 1, Test 60% of AMVC

Similar results were obtained for the test at 60% (Figure 4.7). In this case the MFCV slightly increases at the end of the test, but this could be associated to a larger number of MUs recruited (30 in total).

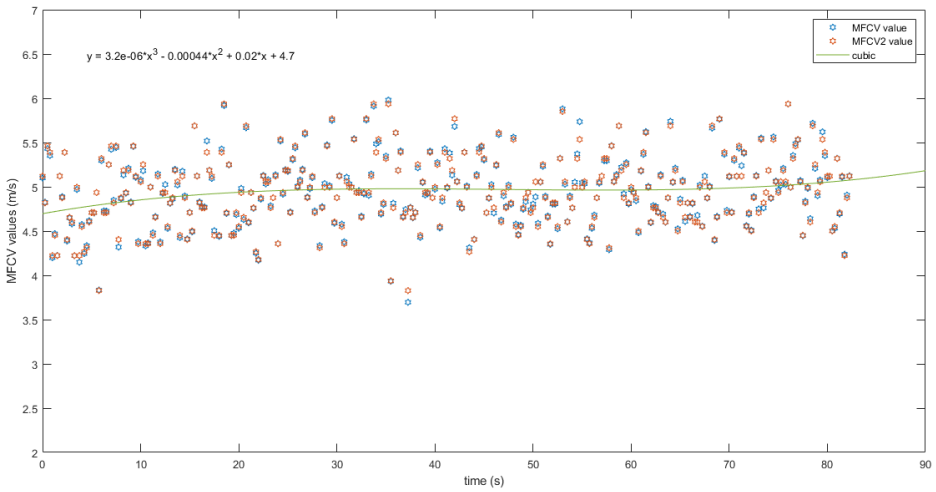

Figure 4.7. MFCV and MFCV2 in test at 60% of AMVC of the first subject. Time evolution of the CVs during the long lasting dorsiflexion.

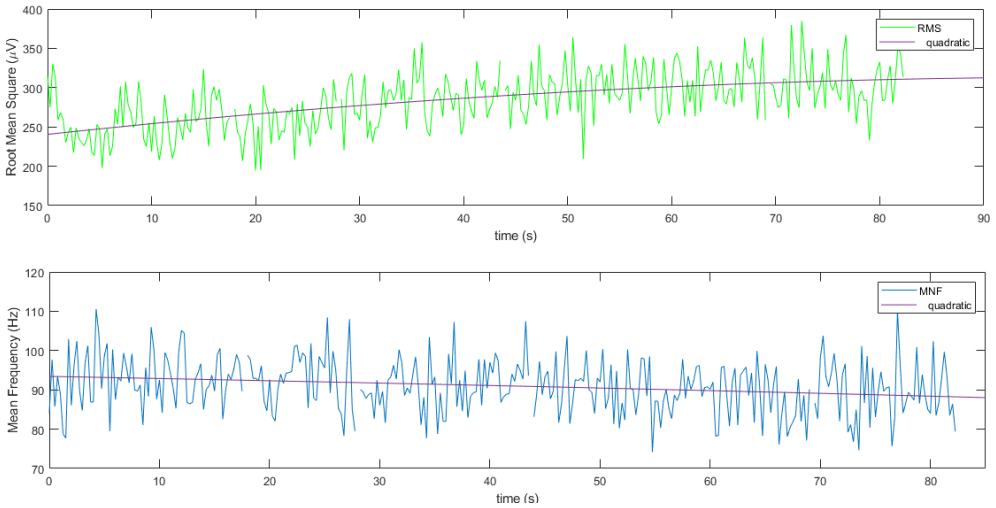

Figure 4.8. EMG descriptors in test at 60% of AMVC of the first subject. First subplot: RMS with quadratic interpolation. Second subplot: MNF with quadratic interpolation.

In fact, even here the fatigue process can be noted from the other EMG descriptors showed in Figure 4.8, that is the increase of the RMS and the decrease in the Mean frequency. Naturally, the RMS amplitude is lower with respect to the test at 80%, and the MNF reaches around 90 Hz with respect to the 55Hz in the test at 80%. Finally, the means (and their standard deviations) of all CVs for each Motor Unit (29 in this test) are shown in the first subplot of Figure 4.9.

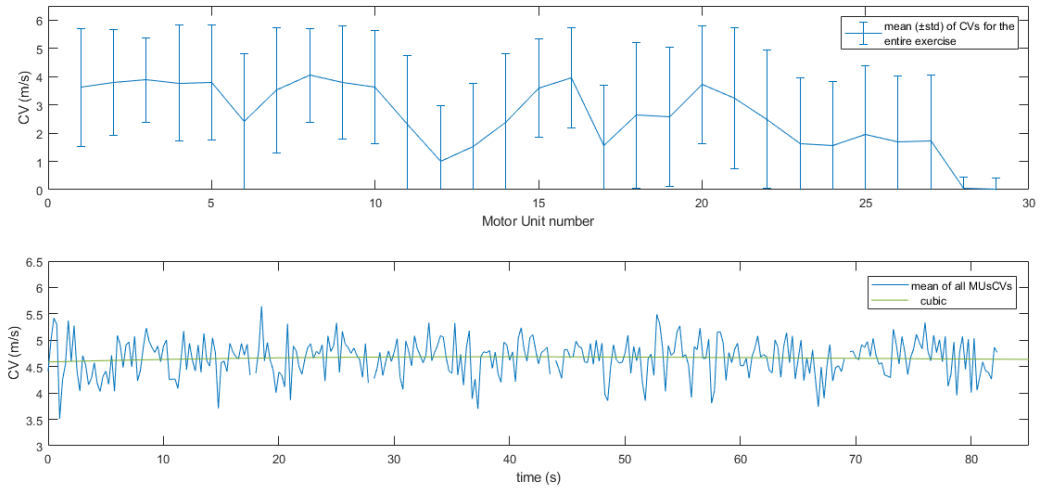

Figure 4.9. MUsCV in test at 60% of AMVC during the LLC dorsiflexion of the first subject. First subplot: mean of all CVs for each Motor Unit. Second subplot: time evolution of CVs mean derived from all MUs at each time instant, with cubic interpolation.

As before, last MUs have a mean value very low or even zero, while the MUs activated from the beginning have a normal mean value. Moreover, in the second subplot, the time evolution of the CV mean is represented. It can be seen that there is not a decrease in the CV, but the value is kept constant at 4.6 m/s, less with respect to the test a 80%. Moreover, as show in table 4.1, there is a good correlation $\rho_1 = 0.6028$ and $\rho_2 = 0.6720$ between MFCV and the mean and median of all MUsCV, respectively, both statistically extremely significant ($p < 0.0001$). Therefore, in this test, from the analysis of the RMS and MNF, it could be said that the process of muscle fatigue is starting. On the other hand, muscle fatigue is not present if we analyze the conduction velocities, neither at muscle fibers' level neither at MUs' level.

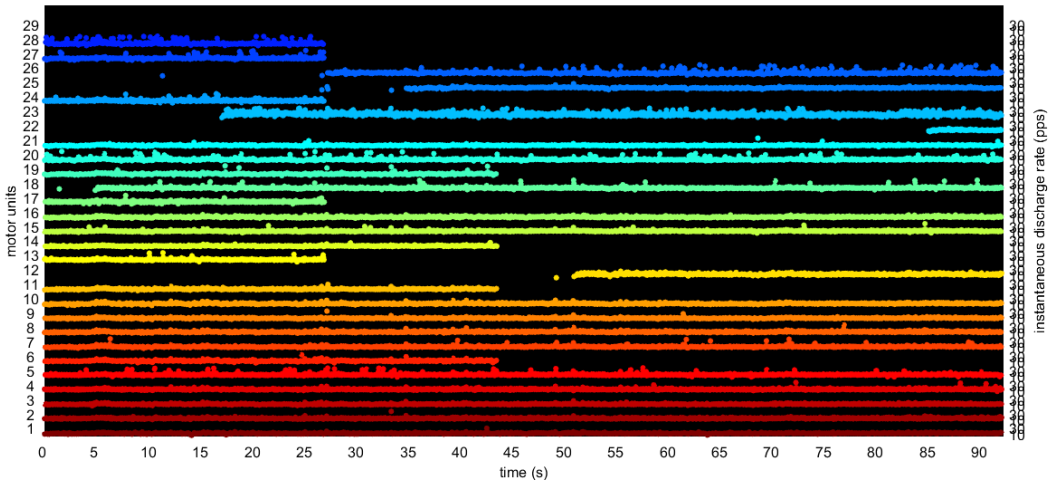

Figure 4.10. MUs firing in test at 60% of AMVC of the first subject.

In Figure 4.10 the firing of all MUs are shown. It can be seen the same process of MUs recruitment described in the test at 80%, where the "holes" represent those time interval in which the MUs were no active.

4.2.2 Repetitive contractions

The second experiment is that of cyclic isometric contractions, where the robot exerted a force for 5 second interspersed with 5 seconds of rest against the subject, causing him to perform a dorsiflexion. Even here, data are extracted from two channels, which were manually selected according to the highest correlation value between signals. Only the results of two subject will be presented, because it came out from data analysis that the EMG signals acquired from three out of five participants were not reliable.

Subject 1, Test 80% of AMVC

Initially, the upsampling method and the Farina method [27] for the time delay were compared. They presented a Pearson coefficient $\rho = 0.9460$ with strong significant evidence $p < 0.0001$. As before, the time evolution of MFCV and MFCV2 are showed in Figure 4.11. In this case, we can notice a time evolution of the CV around the range 4.5-5.2m/s; however, in some time instants the CV takes values within

the range 3-3.5m/s. The global trend is given by cubic interpolation that show the presence of an initial decrease at the end of the experiment. This could represent the beginning of the muscle fatigue process. In fact the other two EMG descriptors, plotted in Figure 4.12, confirmed this hypothesis.

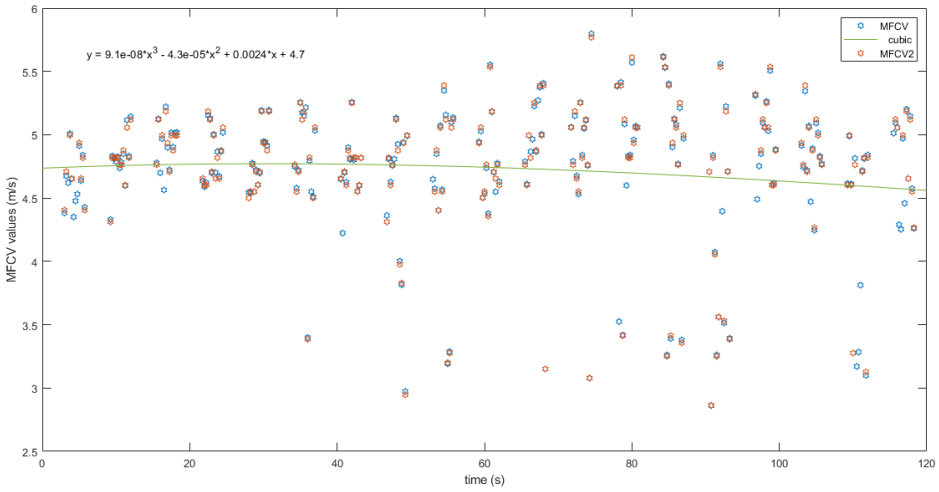

Figure 4.11. MFCV and MFCV2 in test at 80% of AMVC. Time evolution of the CVs during the repetitive dorsiflexions of the first subject.

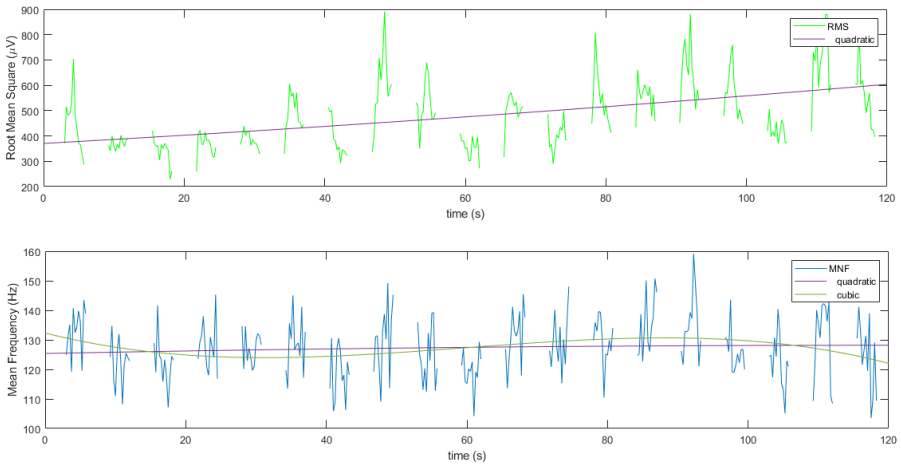

Figure 4.12. EMG descriptors in test at 80% of AMVC during the repetitive dorsiflexions of the first subject. First subplot: RMS with quadratic interpolation. Second subplot: MNF with quadratic interpolation.

It is possible to note that the amplitude of the RMS has a linear increase from the beginning. On the other hand, the linear interpolation in the second subplot of Figure 4.12, that is the MNF plot, is constant along the entire exercise, while the cubic interpolation of the MNF values presents a small frequency spectrum compression around 30 seconds and it starts to decrease at the end of the exercise.

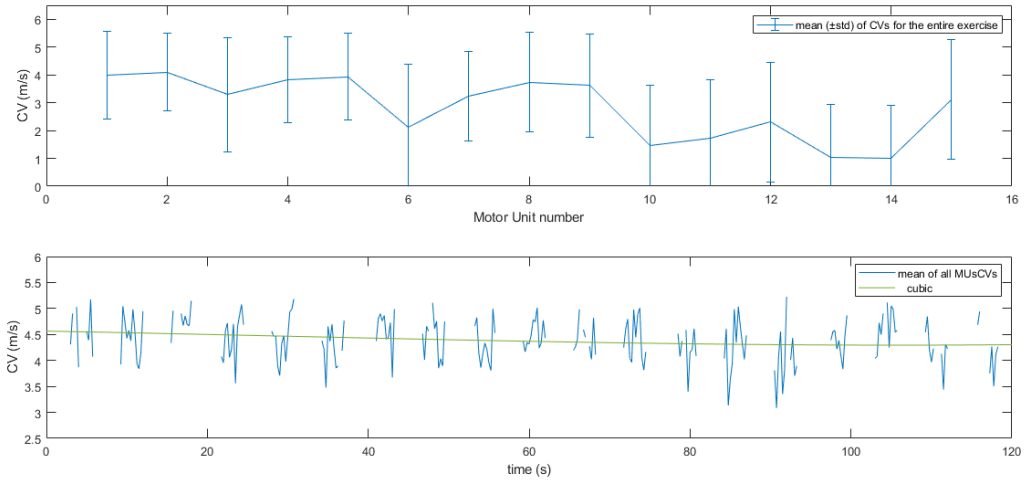

Figure 4.13. MUsCV in test at 80% of AMVC during the repetitive dorsiflexions of the first subject. First subplot: mean of all CVs for each Motor Unit. Second subplot: time evolution of the mean of CV values derived from all MUs at each time instant, with cubic interpolation.

Then, the results of the mean of the CV between all MUs (15 in this test) along the entire exercise present a small decrease at the end of the test, as expected according to the previous experiment (Figure 4.13). Here, a correlation $\rho_1 = 0.4413$ between MFCV and mean, and $\rho_2 = 0.4685$ between MFCV and median was found, both with significant evidence $p < 0.0001$. Moreover, the mean (and the standard deviation) of the CVs for each MU indicate that the initial encountered MUs are more active if compared to the last ones, exactly as in the previous experiments presented. This can be observed even in Figure 4.14, where the MUs firing along the entire exercise are represented for each Motor Unit. Finally, since the subject performing the two experiments was the same, these results have been compared with those obtained from the long-lasting contraction.

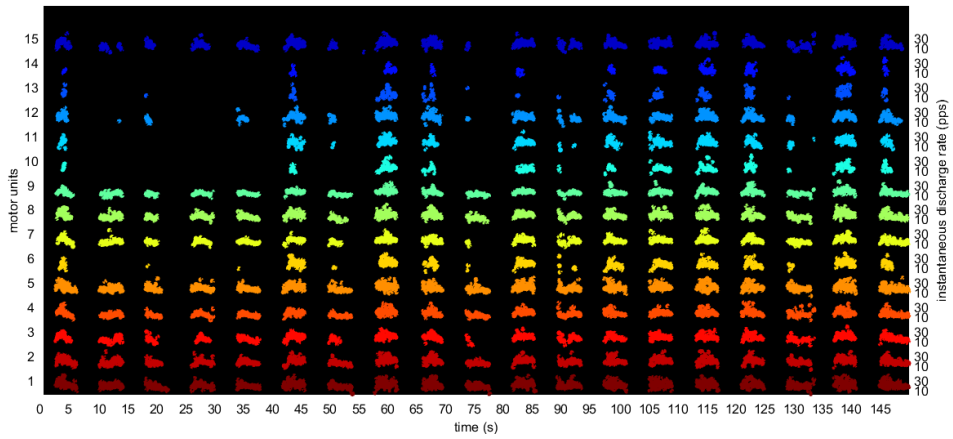

Figure 4.14. MUs firing in test at 80% of AMVC of the first subject.

As it was expected, the value of the MFCV in the long lasting contraction has a value greater than the MFCV during repetitive contractions interspersed with some rest. The same holds even for the other EMG descriptors, as shown in the table 4.2.

Table 4.2. EMG descriptors of the first subject performing the experiment of Long Lasting Contraction (LLC) and the experiment of Repetitive Contractions (RCs).

EMG Descriptors	LLC	RCs
MFCV (start)	5.60 m/s	4.75 m/s
MFCV (end)	4.53 m/s	4.58 m/s
mean MUsCVs (start)	5.11 m/s	4.56 m/s
mean MUsCVs (end)	4.21 m/s	4.32 m/s
RMS (start)	680 μV	370 μV
RMS (end)	800 μV	600 μV
MNF (start)	84 Hz	132 Hz
MNF (end)	55 Hz	122 Hz

Therefore, it is possible to conclude that at the same level of contraction, long lasting exercises more rapidly induce fatigue if compared to repetitive contractions. In fact, from the analysis performed, we found that some rest between each contraction let the fatigue process starts later.

Subject 2, Test 80% of AMVC

The same analysis during repetitive contractions was done for the subject 2. As can be seen in the Figure 4.15 the cubic interpolation of the MFCV, as well as that of MFCV2, increase along the exercise.

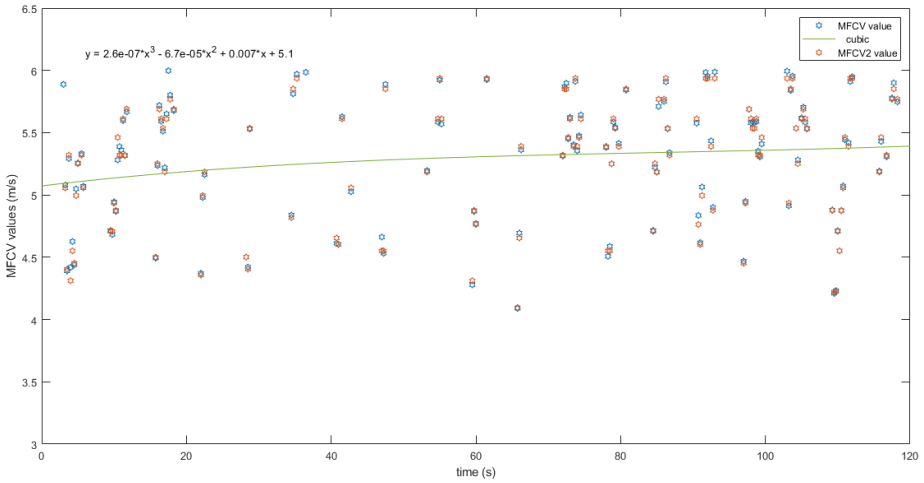

Figure 4.15. MFCV and MFCV2 in test at 80% of AMVC. Time evolution of the CVs during the repetitive dorsiflexions of the second subject.

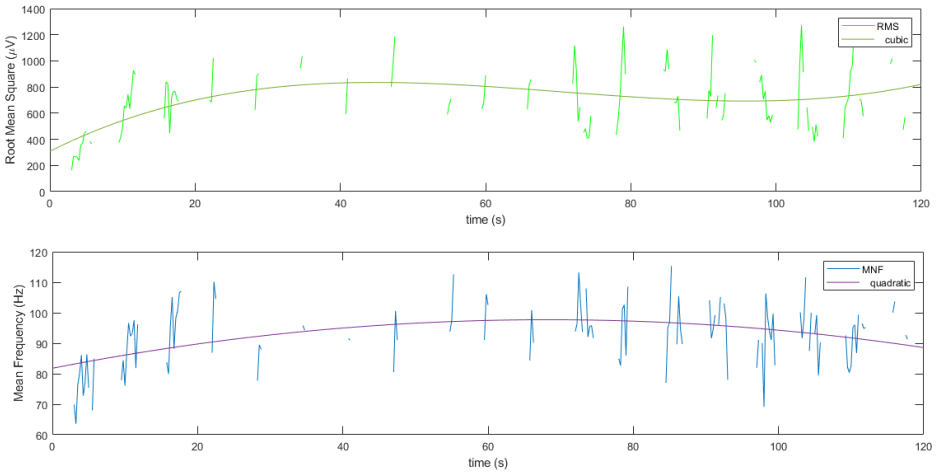

Figure 4.16. EMG descriptors in test at 80% of AMVC during the repetitive dorsiflexions of the second subject. First subplot: RMS with quadratic interpolation. Second subplot: MNF with quadratic interpolation.

This suggested that muscle fatigue was not caused to the specific subject. This is reflected also in the other EMG descriptors, as shown in Figure 4.16, that behave different than they do during the fatigue process. Regarding to the MUs, the same scheme was found in the mean with respect to the MUs number; it means that the MUs, which are activated at the beginning of the exercise, have a CV mean value higher than that of the MUs recruited at the end of the exercise.

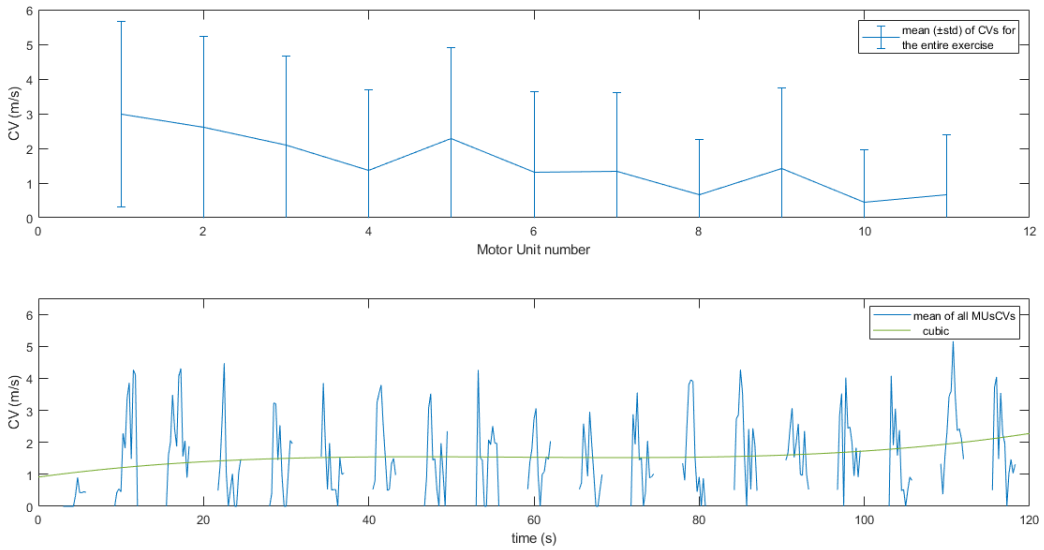

Figure 4.17. MUsCV in test at 80% of AMVC during the repetitive dorsiflexions of the second subject. First subplot: mean of all CVs for each Motor Unit. Second subplot: evolution over time of the mean of CV values derived from all MUs at each time instant, with cubic interpolation.

Subsequently, the time evolution of the mean is showed in the second subplot of Figure 4.17. Exactly as the behaviour of the MFCV, a small increment is encountered at the end of the exercise, showing that the fatigue process is not present. In fact, the MFCV and mean of MUsCV have a correlation $\rho_1 = 0.7366$, while the MFCV and the median have a $\rho_2 = 0.7506$, both with significant evidence $p < 0.0001$.

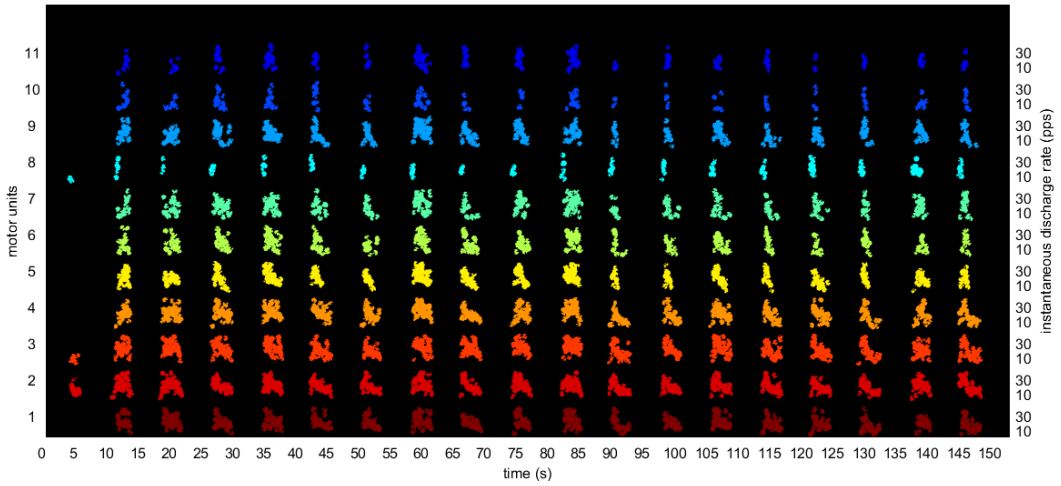

Figure 4.18. MUs firing in test at 80% of AMVC of the second subject.

Finally, as can be noted in Figure 4.18, all MUs are active and fire from the beginning; nevertheless, some of them, e.g. MU_8, MU_{10}, MU_{11} present a small number of firings. This should happen because when the muscles contraction needs higher frequency firing for being kept constant; thus, other MUs are required to fire, giving their MUAPs contributes in order to support the previous ones.

Chapter 5

Conclusions

The idea behind the whole work reflects the goal of a long term project, aimed to improve the adaptive control strategy of the Motorized Ankle Foot Orthosis, by introducing a physiological parameter in the Tacit Adaptability module. This parameter should consider the user's physiological muscle changes over time, and thus it should be an indicator of muscle fatigue. Therefore, this work can be considered as an exploratory study required to evaluate the feasibility of the fatigue assessment technique in the robot-training conditions with healthy individuals. In the first study, three co-contraction indexes have been studied and implemented. Through the use of these indexes, it has been possible to observe the simultaneous activation of an agonist pair of muscle, namely the tibialis anterior and the gastrocnemius medialis. A pattern was identified in the plantarflexion, while an oscillatory behaviour of these CIs was encountered in the dorsiflexion. The scheme that was found could be considered as a good indicator of muscle activation; nevertheless, it was not possible to find a correlation with muscle fatigue. This depended on the amplitude of the signals, that was too low for causing fatigue. In the second study, the conduction velocity was investigated. An innovative High-Density surface EMG technique was employed for the signals acquisition. The DEMUSE was used in order to decompose the signals and extract the Motor Units. The conduction velocity was computed at global level (MFCV) and local level (MUCV). A correlation between these two variables was found in the experiments. In addition, the analysis of the results point out the possibility of using the CV for the estimation of muscle fatigue. The

validation of the results was confirmed by the analysis of other EMG descriptors, which are usually used in the literature. Moreover, it was found that the fatigue process started later in the repetitive contraction exercise, if compared to the long lasting contraction. In fact, some rest between each contraction is shown to be useful to delay the muscle fatigue; this could be very helpful in the choise of the exercise during a rehabilitation therapy. Therefore, a first evaluation of the conduction velocity extracted with HD-sEMG was performed in two exercises, giving proof concept of its possible use for muscle fatigue assessment in the lower limb muscle.

5.1 Future works

The co-contraction indexes showed to be good indicators of muscle co-activation. Nevertheless, other experiments need to be performed at higher levels of contraction in order to investigate a possible relation with the fatigue. In addition, since it is preferable to automatically select the best channels for the CV extraction, the automatic channels selection algorithm, implemented in this work, could be revised and refined. In fact, it should be able to automatically discard CV values outside of the physiological range. Then, being an exploratory study, it was not the goal of this thesis to provide conclusive evidence about the effectiveness of the approach. For this reason, assessing with statistical significance the working hypothesis will certainly require to extend the measures to a higher number of subjects that could be involved in further experiments following the same protocols proposed. Finally, once the fatigue level will be precisely identified through this variable, and once the proposed control strategy is implemented in the ankle orthosis, new empirical measures should be analyzed to assess the benefits of the proposed approach.

Bibliography

[1] OpenStax, “Anatomy & Physiology”, Ch. 10, OpenStax CNX, Feb. 2016, https://opentextbc.ca/anatomyandphysiology/.

[2] J. Barron, “Physiology of Muscles”, Jan. 2013, https://jonbarron.org/article/physiology-muscles.

[3] W. R. Frontera and J. Ochala, “Skeletal Muscle: A Brief Review of Structure and Function”, Calcified Tissue Intern., 96(3), 183-195, 2014.

[4] R. Merletti and P. Parker, “Electromyography: physiology, engineering and noninvasive applications”, Ch. 1,2,4-7,9,10,12 2004.

[5] A. Del Vecchio, F. Negro et al., “Distribution of muscle fiber conduction velocity for representative samples of motor units in the full recruitment range of the tibialis anterior muscle.”, Vol. 222, Issue2, Feb. 2018.

[6] R. Merletti and D. Farina, “Surface Electromyography, Physiology, Engineering and Applications”, Ch. 1-5,7,10, Inst. of Electric. and Electron. Eng., Inc. 2016.

[7] E. Henneman, “Recruitment of motoneurons: the size principle.” Progr. in Clin. Neuroph., Vol. 9, 1981.

[8] R. E. Burke, “Handbook of physiology - The nervous system II, Motor units: anatomy, physiology, and functional organization”, Ch.10, Arkose Press, 2015.

[9] A. W. Mitchell, “Understanding EMG”, Oxford University Press 2013.

[10] J. S. Petrofsky et al., “Evaluation of the amplitude and frequency components of the surface EMG as an index of muscle fatigue.”, Erg. 25(3), 213-223, 1982.

[11] D. Staudenmann et al., “Increase in heterogeneity of biceps brachii activation during isometric submaximal fatiguing contractions: a multichannel surface EMG study”, J Neuroph. 111: 984-990, 2014.

[12] K. Marri and R. Swaminathan, “Classification of Muscle Fatigue in Dynamic Contraction Using Surface Electromyography Signals and Multifractal Singularity Spectral Analysis”, J. Dyn. Sys. Meas. Control 138(11), 2016.

[13] D. Farina, M. Pozzo et al., “Assessment of Average Muscle Fiber Conduction Velocity From Surface EMG Signals During Fatiguing Dynamic Contractions”, IEEE Trans. on Biom. Eng., VOL. 51, No. 8, 2004.

[14] D. Farina and D. Falla, “Estimation of muscle fiber conduction velocity from two-dimensional surface EMG recordings in dynamic tasks”, Biom. Sig. Proc. and Control 3, 138-144, 2008.

[15] G. Marco et al., “Surface EMG and muscle fatigue: multi-channel approaches to the study of myoelectric manifestations of muscle fatigue”, Physiol., 2017.

[16] R. Merletti et al., “Myoelectric manifestations of fatigue in voluntary and electrically elicited contractions”, J. Appl. Physiol. 69 1810-20, 1990.

[17] G. Kim, M. Ahad et al., “Correlation of muscle fatigue indices between intramuscular and surface EMG signals”, IEEE Proc. 2007.

[18] J. B. Fernando et al., “Estimation of muscle fatigue by ratio of mean frequency to average rectified value from surface electromyography”, IEEE Eng. Bio. Med. and Soc., 2016.

[19] T. Sadoyama, T. Masuda et al., “Fibre conduction velocity and fibre composition in human vastus lateralis", Eur. J. Appl. Physiol., 57:767-771, 1988.

[20] D. Farina and R. Merletti, “A novel approach for estimating muscle fiber conduction velocity by spatial and temporal filtering of surface EMG signals”, IEEE Trans. Biom. Eng., vol. 50, no. 12, pp. 1340-1351, 2003.

[21] D. Farina and R. Merletti, "Methods for estimating muscle fiber conduction velocity from surface electromyographic signals", Med. Biol. Eng. Comput., vol. 42, pp. 432-445, 2004.

[22] W. H. J. P. Linssen, D. F. Stegeman et al., "Force and fatigue in human type I muscle fibers", Brain, vol. 114, pp. 2123-2132, 1991.

[23] M. M. Lowery, C. L. Vaughan et al., "Spectral compression of the electromyographic signal due to decreasing muscle fiber conduction velocity", IEEE Trans. Rehab. Eng., vol. 8, no. 3, pp. 353-361, Sep. 2000.

[24] R. B. J. Beck, C. J. Houtman, et al., "A Technique to Track Individual Motor Unit Action Potentials in Surface EMG by Monitoring Their Conduction Velocities and Amplitudes", IEEE Trans. on Biom. Eng., Vol. 52, No. 4, 2005.

[25] R. B. Beck, M. J. O'Malley et al., "Tracking Motor Unit Action Potentials in the Tibialis Anterior during fatigue", Muscle Nerve 32: 506 -514, 2005.

[26] D. Farina, E. Fortunato and R. Merletti, "Noninvasive Estimation of Motor Unit Conduction Velocity Distribution Using Linear Electrode Arrays", IEEE Trans. on Biom. Eng., Vol. 47, N. 3, 2000.

[27] D. Farina, W. Muhammad et al., "Estimation of single motor unit conduction velocity from surface electromyogram signals detected with linear electrode arrays", Med. Biol. Eng. Comput. 39: 225, 2001.

[28] D. Farina and A. Holobar, Characterization of Human Motor Units From Surface EMG Decomposition, Vol. 104, No. 2, 2016.

[29] M. Gazzoni, D. Farina and R. Merletti, "A new method for the extraction and classification of single motor unit action potentials from surface EMG signals", J. Neurosci. Methods.,Jul 30;136(2):165-77, 2004.

[30] A. Holobar, D. Zazula, "Gradient Convolution Kernel Compensation Applied to Surface Electromyograms", ICA 2007, LNCS 4666, pp. 617-624, 2007a.

[31] A. Holobar and D. Zazula, "Multichannel Blind Source Separation Using Convolution Kernel Compensation", IEEE Tr. Sig. Proc. 55 (9), 4487-4496, 2007b.

[32] F. Negro et al., "Multi-channel intramuscular and surface EMG decomposition by convolutive blind source separation," J. of Neur. Eng., Vol. 13, n. 2, 2016.

[33] S. De Giorgi, "Evaluation of High-Density EMG Feature Extraction and Selection to Recognize Lower Limbs Movements for a Rehabilitation Exoskeleton", Master thesis, Politecnico di Torino, 2017-2018 .

[34] M. Barbero, R. Merletti, A. Rainoldi, "Atlas of Muscle Innervation Zones, Understanding Surface Electromyography and Its Applications", 2012.

[35] G. Piervirgili et al., "A new method to assess skin treatments for lowering the impedance and noise of individual gelled Ag-AgCl electrodes", Phys. Meas. 2014.

[36] K. Nishihara and T. Isho, "Location of Electrodes in Surface EMG, EMG Methods for Evaluating Muscle and Nerve Function", 2012.

[37] H. C. Rubana et al., "Surface electromyography signal processing and classification techniques", Sensor(Basel), vol. 13(9), pp. 12431-12466, 2013.

[38] H. Tam and J. G. Webster, "Minimizing Electrode Motion Artifact by Skin Abrasion",Trans. on Biom. Eng., vol. 24, 1977.

[39] T. Bacek, M. Moltedo, K. Langlois, G. A. Prieto, M. C. Sanchez-Villamañan, J. Gonzalez-Vargas, B. Vanderborght, D. Lefeber and J. C. Moreno, "BioMot Exoskeleton - Towards a Smart Wearable Robot for Symbiotic Human-Robot Interaction", 2017 International Conference on Rehabilitation Robotics (ICORR) QEII Centre, London, UK, July 17-20, 2017.

[40] M. Bortole, J. C. Moreno et al., "The H2 robotic exoskeleton for gait rehabilitation after stroke: early findings from a clinical study", J. N. Reh., 2015.

[41] S. Shimoda et al., "Joint stiffness tuning of exoskeleton robot H2 by tacit learning". Intern. Workshop on Symb. Inter., Springer pp. 138-144, 2015.

[42] V. Grosu et al., "Design of smart modular variable stiffness actuators for robotic assistive devices", Trans. on Mechatr., 2017.

[43] R. Van Ham, "Compliant Actuation for Biologically Inspired Bipedal Walking Robots", Phd thesis dissertation, Brussels, July 2006.

[44] M. Moltedo et al., "Mechanical Design of a Lightweight Compliant and Adaptable Active Ankle Foot Orthosis", IEEE Biom. BioRob, 2016.

[45] D. F. Stegeman and J. Hermens, "Standards for suface electromyography: The European project Surface EMG for non-invasive assessment of muscles (SENIAM)", 2007. http://www.seniam.org/

[46] S. Shimoda and H. Kimura, "Neural computation scheme of compound control: Tacit learning for bipedal locomotion", Control, vol. 1, n. 4, pp. 275-283, 2008.

[47] S. Shimoda and H. Kimura, "Bio-mimetic Approach to Tacit Learning based on Compound Control", IEEE Trans. on Sys., B, vol. 40, no. 1, pp. 77-90, 2010.

[48] S. Shimoda et al., "Stability analysis of tacit learning based on environmental signal accumulation", IEEE/RSJ Intern. Conf. on Intel. Rob. and Sys., 2012.

[49] S. Shimoda et al., "Adaptability of Tacit Learning in Bipedal Locomotion", IEEE Trans. on aut. mental develop., Vol. 5, No. 2, 2013.

[50] G. A. Prieto et al., "Tacit Adaptability of a Mechanically Adjustable Compliance and Controllable Equilibrium Position Actuator, a Preliminary Study", from book: Wearable Robotics: Challenges and Trends: Proceedings of the 2nd International Symposium on Wearable Robotics, WeRob2016, 2016.

[51] G. A. Prieto et al., "Feasibility of submaximal force control training for robot-mediated therapy after stroke", drom book: Biosystems & Biorobotics, vol 21, pp. 256-260, Springer, ICNR 2018.

[52] https://www.otbioelettronica.it/index.php?lang=en

[53] OT BioLab UserManual v3.3 for software version 2.0.6479.0.

[54] A. Holobar, "Decomposition of Multichannel Surface Electromyograms (DEMUSE), Marie Curie Intra-European Fellowship, 6^{th} EU Framework Programme, 2007. http://www.lisin.polito.it/DEMUSE.

[55] "DEMUSE tool - user manual Version 4.1".

[56] A. Holobar, M. A. Minetto and D. Farina, "A signal-based approach for assessing the accuracy of high-density surface EMG decomposition", IEEE/EMBS Conference on Neural Engineering (NER), 2013.

[57] S. Al-Qaisia and F. Aghazadehb, "Electromyography analysis: Comparison of maximum voluntary contraction methods for anterior deltoid and trapezius muscles", Proc. Man. 3, pp. 4578-4583, 2015.

[58] M. D. Lewek et al., "Knee stabilization in patients with medial compartment knee osteoarthritis", Arthritis Rheum., 52(9):2845-53., 2005.

[59] O.S. Mian,J. M. Thom et al., "Metabolic cost, mechanical work, and efficiency during walking in young and older men", Arthritis Rheum., 52(9):2845-53, 2005.

[60] D. A. Winter, "Biomechanics and motor control of Human Movement", Chapter 10, pp. 269-273, Wiley 2009.

[61] B. A. Knarr, J. A. Zeni Jr and J. S. Higginson, "Comparison of electromyography and joint moment as indicators of co-contraction". J. Electromy. Kin. 2012.

[62] R. Osu, D. W. Franklin, et al., "Short- and Long-Term Changes in Joint Co-Contraction Associated With Motor Learning as Revealed From Surface EMG", J. Neurophysiol 88: pp. 991-1004, 2002.

[63] E. Kellis et al, "Muscle co-activation around the knee in drop jumping using the co-contraction index", J. of Electr. and Kin. 13. pp. 229-238, 2003.

[64] K.S. Rudolph, M. J. Axe et al., "Dynamic stability in the anterior cruciate ligament deficient knee", Knee Surg, Sports Traumatol, Arthrosc, 9:62-71, 2001.

[65] K. Falconer and D. Winter, "Quantitative assessment of cocontraction at the ankle joint during walking", Electromy. Clin. Neurophys. 25, 135-149, 1985.

[66] Y. Iwamoto et al., "Differences of muscle co-contraction of the ankle joint between young and elderly adults during dynamic postural control at different speeds", J. Phys. Anthrop. 2017.

[67] G. Frost, J. Dowling et al., "Cocontraction in three age groups of children during treadmill locomotion", J. Electromyogr. Kinesiol. 7, 179-186, 1997.

[68] V.B. Unnithan, J. Dowling, et al., "Cocon- traction and phasic activity during gait in children with cerebral palsy", Electromy. Clin. Neurophy., 487-494, 1996.

[69] E. S. Gardinier, "The relationship between muscular co-contraction and dynamic knee stiffness in ACL-deficient non-copers", bachelor thesis, 2009.

[70] N. Ahmada, Z. Taha and P. L. Eu, "Energetic requirement, muscle fatigue, and musculoskeletal risk of prolonged standing on female Malaysian operators in the electronic industries: influence of age", Vol.1, No 2, pp 47-580, 2006,

[71] K. McGill and L. Dorfman, "High resolution alignment of sampled waveforms", IEEE Trans. Biom. Eng., 31:462-70, 1984.

[72] I. W. Hunter, R. E. Kearney and L. A. Jones, "Estimation of the conduction velocity of muscle action potentials using phase and impulse response function techniques", Med Biol Eng Comp, 25:121-6, 1987.

[73] D. Farina, E. Fortunato and R. Merletti, "Noninvasive estimation of motor unit conduction velocity distribution using linear electrode arrays", IEEE Trans. on Biom. Eng., 47(3), 380-388, 2000.

[74] W. Muhammad et al., "Comparison of single and multiple time delay estimators: application to muscle fiber conduction velocity estimation", RR-0015, 2000.

[75] User Manual v1.4 Quattrocento, "Bioelectrical signal amplifier".

[76] V. V. Tscharner, "Muscle Fiber Conduction Velocity", Encyclopedia of Neuroscience, pp. 2262-2265, 2006.

[77] D. Gagnon, A. B. Arsenault et al., "Cocontraction changes in muscular fatigue at different levels of isometric contraction", Intern. J. of Ind. Erg 9(4), pp. 343-348, 1992.